

Finite-temperature properties of string-net models

Anna Ritz-Zwilling,^{1,*} Jean-Noël Fuchs,^{1,†} Steven H. Simon,^{2,‡} and Julien Vidal^{1,§}

¹*Sorbonne Université, CNRS, Laboratoire de Physique Théorique de la Matière Condensée, LPTMC, F-75005 Paris, France*

²*Rudolf Peierls Centre for Theoretical Physics, Oxford, OX1 3PU, United Kingdom*

We consider a refined version of the string-net model which assigns a different energy cost to each plaquette excitation. Using recent exact calculations of the energy-level degeneracies we compute the partition function of this model and investigate several thermodynamical quantities. In the thermodynamic limit, we show that the partition function is dominated by the contribution of special particles, dubbed pure fluxons, which trivially braid with all other (product of) fluxons. We also analyze the behavior of Wegner-Wilson loops associated to excitations and show that they obey an area law, indicating confinement, for any finite temperature except for pure fluxons that always remain deconfined. Finally, using a recently proposed conjecture, we compute the topological mutual information at finite temperature, which features a nontrivial scaling between system size and temperature.

I. INTRODUCTION

Topological quantum phases of matter are characterized by various properties that are robust against small perturbations (see Ref. [1] for a review). In two dimensions, the most famous examples are the chiral phases associated with the fractional quantum Hall effect [2]. One of the main features of these topologically ordered phases is the nontrivial quantum statistics of quasiparticles, called anyons [3–7], which have recently been studied in several experiments [8–11]. The robustness of these phases and the exotic braiding properties of anyons make them very good candidates for quantum memories and topological quantum computing (see Refs. [12] and references therein).

To analyze topologically ordered phases, it is often useful to consider exactly solvable models such as the toric code model [13] or the string-net (SN) model [14], to name but a few. Interestingly, these models can now be simulated using different quantum artificial devices. For instance, the toric code model has been implemented using superconducting qubits [15–18] or Rydberg atoms held in optical tweezers [19, 20], whereas the SN model has very recently been designed via a superconducting quantum processor [21]. The aforementioned models are considered as the paradigmatic models of topological phases. The corresponding Hamiltonians are made of local commuting projectors and, as such, they only generate a particular class of topological phases known as achiral (vanishing Hall conductance) and doubled [22, 23].

Although topological quantum order is stable against local perturbations [24] at zero temperature ($T = 0$), it may be very fragile in the presence of thermal fluctuations ($T \neq 0$). In two dimensions, it has even been

shown that, for any Hamiltonian build from local commuting projectors, topological order is destroyed in the thermodynamic limit for any $T > 0$ [25]. Nevertheless, a subtle interplay between the system size and the temperature allow to consider a size-dependent temperature below which the topological order is preserved (see, e.g., Refs. [26, 27] for a discussion of the toric code model). This problem of thermal fragility is especially important in the perspective of using these systems to realize self-correcting memories [28–31].

In the present paper, we study a refined version of the SN model and study its finite-temperature properties. In recent years, several generalizations of the SN model have been proposed [32–35]. These generalizations allow one to consider any input unitary fusion category (UFC) \mathcal{C} and hence, to generate all possible achiral phases. These emergent achiral topological phases are described by the Drinfeld center of \mathcal{C} , $\mathcal{Z}(\mathcal{C})$, which is a unitary modular tensor category, i.e., a well-behaved anyon theory. Akin to quantum double models [13], SN models have two types of excitations corresponding to violations of either vertex constraints or plaquette constraints. Nevertheless, by construction, SN models cannot create pure vertex excitations. In other words, when a vertex is excited, neighboring plaquettes are also automatically excited [this problem can be circumvented by adding extra degrees of freedom (tails) giving rise to the so-called extended SN models [36]]. Here, as originally proposed by Levin and Wen [14], we restrict to the Hilbert space satisfying the vertex constraints (the branching rules) so that only plaquette excitations are allowed (see Sec. II), but we propose a refinement of the SN model by assigning a different energy cost to each possible plaquette excitation (a similar extension has been already discussed for quantum double models in Ref. [37]). Using our recent exact calculations of the energy-level degeneracies [38], we compute various quantities at finite temperature in this refined string-net (RSN) model which encompasses, as special cases, the original SN model and its generalizations [32–35]. In particular, we compute the partition

* anna.ritz_zwilling@sorbonne-universite.fr

† jean-noel.fuchs@sorbonne-universite.fr

‡ steven.simon@physics.ox.ac.uk

§ julien.vidal@sorbonne-universite.fr

function, the energy, specific heat, and the entropy (see also Ref. [39] for related works), as well as the Wegner-Wilson loops (for contractible and noncontractible contours), and the topological mutual information. Importantly, we show that, while the Drinfeld center $\mathcal{Z}(\mathcal{C})$ is enough to describe the ground state of the system, additional information is needed at finite temperature, namely the internal multiplicities of the anyons, which depend on the input category \mathcal{C} and are obtained from the tube algebra. Among simple objects of $\mathcal{Z}(\mathcal{C})$, we identify subsets that play special roles and depend on \mathcal{C} : the fluxons \mathcal{F} (i.e. single plaquette excitations), a particular subset of the fluxons, which we call *pure fluxons* \mathcal{P} , and the fusion product of fluxons, notated \mathcal{F}^\otimes .

The article is organized as follows. We first review the construction of SN models (Sec. II) and introduce a generalization (RSN) that lifts all nontopological degeneracies in the energy spectrum. Then, we review the results on energy-level degeneracies that were obtained in [38] and add the case of a punctured manifold (Sec. III). Next, we compute the partition function (Sec. IV) and analyze the resulting equilibrium thermodynamics (Sec. V C). In Sec. VI, we compute the thermal average of projectors onto given quasiparticle sectors in a given region. Using these results for projectors, it is straightforward to compute the thermal average of Wegner-Wilson loops and to discuss the confinement of quasiparticles (Sec. VII). Then, we study entanglement properties by focusing on the topological mutual information at finite temperature (Sec. VIII). In Sec. IX, we conclude and give perspectives. Appendices provide details on the notions of fluxons (Appendix A), on the fusion of simple objects of the Drinfeld center as obtained from the tube algebra (Appendix B), and on a surgery approach to computing the degeneracies (Appendix C).

II. STRING-NET MODELS

The original SN model has been introduced by Levin and Wen [14] and generalized in Refs [32–35] in order to consider any UFC as input category. In the following, we briefly recall the basic ingredients of this model and we refer the interested reader to Ref. [35] for a more complete and detailed introduction (see also Ref. [38] for a brief overview). Below, we shall propose another extension of the SN models, which can also be defined for any UFC. In some sense, it is a “refined generalized” SN model but for simplicity, we will just call it RSN model.

A SN model is built from a UFC \mathcal{C} whose fusion rules define the Hilbert space of the system. It is defined on a two-dimensional trivalent graph. Here, for simplicity, we consider a trivalent graph with N_p plaquettes embedded on an orientable closed surface. The case of surfaces with boundaries is discussed in Ref. [38] and subtleties arising for nonorientable surfaces are addressed, e.g., in Refs. [40, 41].

A basis for the Hilbert space is obtained by assigning

a quantum number a, b, c, \dots to each directed edge of the graph. These microscopic degrees of freedom are chosen as simple objects of the category \mathcal{C} . In some cases, extra quantum numbers may also be assigned to vertices. The UFC is equipped with fusion multiplicity coefficients N_{abc} (sometimes written in the form of a matrix N_a with rows b and columns c) which give the number of ways that a, b, c can fuse to the identity. That is, if a, b, c meet at a vertex (inwardly directed) and fuse to the identity, then the vertex is given a quantum number which ranges from 1 to N_{abc} . If a, b, c do not fuse to the identity, then $N_{abc} = 0$.

In the present work, we restrict the Hilbert space to basis states satisfying the fusion rules at each trivalent vertex. In other words, we exclude vertex configurations with $N_{abc} = 0$.

A. String-net model

Within the restricted Hilbert space \mathcal{H} , the original Hamiltonian of the SN model is given by [14]:

$$H = - \sum_{p=1}^{N_p} B_p, \quad (1)$$

where B_p ’s are local commuting projectors acting on the plaquette p . The ground-state manifold is generated by all states $|\psi\rangle$ such that $B_p|\psi\rangle = |\psi\rangle$ for all plaquettes p . Excited states are obtained by violating this plaquette constraint. Elementary excitations can thus be seen as plaquette excitations and are dubbed fluxons [38]. For a given input UFC \mathcal{C} , these fluxons belong to a subset \mathcal{F} of the simple objects of the so-called Drinfeld center $\mathcal{Z}(\mathcal{C})$ (by convention, we also include the vacuum $\mathbf{1}$ in this subset although it does not cost any energy). Hence, B_p can be interpreted as the projector onto the vacuum of $\mathcal{Z}(\mathcal{C})$, inside the plaquette p . The excitation energy of a plaquette containing a fluxon $A \neq \mathbf{1}$ is set to 1. Note that, because of the vertex constraint, some objects of $\mathcal{Z}(\mathcal{C})$ may not be generated even by multiple fusion of fluxons (see Sec. III C).

B. Refined string-net model

Actually, one can consider a refined version of the SN model by assigning to each plaquette p , a hermitian coupling matrix \mathcal{J}_p^A , which depends on the fluxon type A and whose row and column indices a, b correspond to internal multiplicity indices. The notion of an internal multiplicity is only relevant for noncommutative UFCs where a fluxon A may carry a multiplicity index a running from 1 to $n_{A,1} > 1$ [38]. In the commutative case, one always has $n_{A,1} = 1$ for fluxons (and 0 otherwise).

The RSN Hamiltonian is then given by:

$$H = - \sum_{p=1}^{N_p} \sum_{A \in \mathcal{F}} \sum_{a,b=1}^{n_{A,1}} \mathcal{J}_p^{A,ab} B_p^{A,ab}, \quad (2)$$

where $B_p^{A,ab}$ acts in the $n_{A,1}$ -dimensional internal space of fluxon A in the plaquette p . When $a = b$, this operator corresponds to the simple idempotent (projector) $p_A^{11,aa}$ of the tube algebra in the 11 sector, acting in the plaquette p . Similarly, when $a \neq b$, $B_p^{A,ab}$ corresponds to the nilpotent $p_A^{11,ab}$ in the 11 sector (see Ref. [38] for more details), acting in the plaquette p . The matrix elements of the operators $B_p^{A,ab}$ in the edge basis can be computed using the tube algebra (see, e.g., Refs. [32, 38]). The fact that we only consider operators acting in the 11 sector is simply due to the vertex constraints (Gauss law) which are always satisfied in the restricted Hilbert space.

For the vacuum $A = \mathbf{1}$, which has no internal multiplicity ($n_{\mathbf{1},1} = 1$), the corresponding projector is the same as the one introduced in Eq. (1) ($B_p^{\mathbf{1},11} = B_p$). The SN model is then recovered by choosing $\mathcal{J}_p^{A,ab} = \delta_{A,1}$, for all p 's. We stress that other choices of $\mathcal{J}_p^{A,ab}$ may lead to ground states with nontrivial fluxons.

In the following, only the eigenvalues of the matrix \mathcal{J}_p^A will appear and will be called $J_p^{A,a}$ where a runs from 1 to $n_{A,1}$. In the basis that diagonalizes the coupling matrix, the Hamiltonian (2) can be rewritten as a sum of local commuting projectors (see also Appendix D of Ref. [38]) and therefore remains exactly solvable. A key feature of the RSN Hamiltonian is that, generically, it has only topological degeneracies. The nontopological degeneracies that may arise in the SN model for noncommutative UFCs (see Ref. [38]) are indeed due to the very specific choice of couplings discussed above.

III. BASIC PROPERTIES OF DEGENERACIES

In this section, we review some important results about the eigenstate topological degeneracies presented in Ref. [38] and extend these to the case of surfaces with punctures. Let us consider a RSN model defined on a trivalent graph with N_p plaquettes embedded on an orientable closed surface of genus g . An eigenstate of H defined in Eq. (2) can be represented by a fusion diagram (see Fig. 1). In this picture, each directed line is related to a fluxon A_p with a multiplicity index a_p and each vertex having three incident edges $A, B, C \in \mathcal{Z}(\mathcal{C})$ is labeled with an integer (not shown) ranging from 1 to N_{ABC} (labelings with $N_{ABC} = 0$ are not allowed), where N_{ABC} 's are the fusion multiplicity coefficients of the Drinfeld center. Such a fusion diagram implicitly assumes that the overall fusion product is the vacuum $\mathbf{1}$.

As discussed in Ref. [38], for a given fluxon configuration $\{A_1, A_2, \dots, A_{N_p}\} \in \mathcal{F} \subseteq \mathcal{Z}(\mathcal{C})$, with multiplicity indices $\{a_1, a_2, \dots, a_{N_p}\}$, the degeneracy of the energy

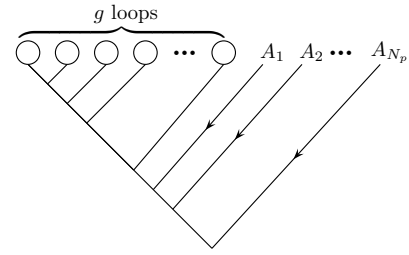


FIG. 1. Fusion tree indicating the topological degeneracy for N_p plaquettes having fluxons A_1, \dots, A_{N_p} on a genus g surface. For clarity, the internal multiplicity index a_i associated with A_i 's and the fusion multiplicity index associated with each vertex are not displayed here.

level,

$$E = - \sum_{p=1}^{N_p} J_p^{A_p, a_p}, \quad (3)$$

is given by counting all possible labelings of the unlabeled lines and vertices in Fig. 1. It is important to note that this (topological) degeneracy only depends on the fusion rules of the Drinfeld center objects but not on the internal multiplicities. We emphasize that extra (nontopological) degeneracies may emerge for fine-tuned couplings as is the case for the SN Hamiltonian given in Eq. (1) [38].

A. Digression on fusion

As explained above, an inwardly directed trivalent vertex A, B, C in a fusion diagram such as Fig. 1 is described by a quantum number ranging from 1 to N_{ABC} . One particular case is when one of the edges is already in the vacuum state $\mathbf{1}$. Then, the two other edges must be in states A and \bar{A} , where \bar{A} is the dual of the object A , i.e., $N_{A\bar{B}\mathbf{1}} = \delta_{B,\bar{A}}$. Graphically, one can go from A to \bar{A} by reversing the orientation of the corresponding edge. Therefore, an equivalent notation for N_{ABC} is $N_{AB}^{\bar{C}}$, where the emphasis is put on the fact that two incoming edges A and B fuse into an outwardly directed edge \bar{C} .

In the following, we will use the notation

$$N_{B_1 B_2 B_3 \dots B_m}^X = \sum_{\substack{Y_1, \dots, Y_{m-2} \\ \in \mathcal{Z}(\mathcal{C})}} N_{B_1 B_2}^{Y_1} N_{Y_1 B_3}^{Y_2} \dots N_{Y_{m-3} B_{m-1}}^{Y_{m-2}} N_{Y_{m-2} B_m}^X, \quad (4)$$

to notate the total number of ways that m objects B_1, \dots, B_m can fuse to X . This N symbol is symmetric under exchange of any of the lower indices. We can also raise and lower indices as follows:

$$N_{B_1 B_2 \dots B_m}^X = N_{B_1 B_2 \dots B_m \bar{X}}^{\mathbf{1}} = N_{\bar{X} B_2 \dots B_m}^{\bar{B}_1}. \quad (5)$$

Finally, we can paste together fusion trees with respective fusion outcomes X and \bar{X} by using the following relation:

$$N_{B_1 B_2 \dots B_m}^1 = \sum_{X \in \mathcal{Z}(\mathcal{C})} N_{B_1, \dots, B_p}^X N_{B_{p+1}, \dots, B_m}^{\bar{X}}. \quad (6)$$

B. Topological degeneracies

Using the notation introduced in (4), we can compute the topological degeneracy of states for a genus g , N_p plaquettes system with fluxons A_1, \dots, A_{N_p} through the plaquettes as:

$$\dim(g; A_1, \dots, A_{N_p}) = \sum_{B_1, \dots, B_g \in \mathcal{Z}(\mathcal{C})} N_{B_1 B_2 \bar{B}_2 \dots B_g \bar{B}_g A_1 A_2 \dots A_{N_p}}^1. \quad (7)$$

This form, which corresponds to the fusion tree of Fig. 1, is given in Ref. [38] and is also re-derived in Appendix C.

We can greatly simplify expressions of this sort using the Verlinde formula [42]

$$N_{A, B}^C = \sum_{D \in \mathcal{Z}(\mathcal{C})} \frac{S_{A, D} S_{B, D} S_{C, D}^*}{S_{1, D}}, \quad (8)$$

where S is the modular S -matrix of the Drinfeld center $\mathcal{Z}(\mathcal{C})$.

Using this form along with the fact that S is unitary and symmetric, one obtains the Moore-Seiberg-Banks result [43]:

$$\dim(g; A_1, \dots, A_{N_p}) = \sum_{C \in \mathcal{Z}(\mathcal{C})} \left[\prod_{p=1}^{N_p} S_{A_p, C} \right] S_{1, C}^{2-2g-N_p}. \quad (9)$$

C. Degeneracies from punctured surfaces

We now cut a disk out of the surface and calculate the effective dimension (degeneracy) of this partial surface, allowing for a particular quantum number of “flux” $X \in \mathcal{Z}(\mathcal{C})$, potentially different from the vacuum and *not necessarily a fluxon* to be coming out of the hole as shown in Fig. 2. If this object has N_p plaquettes plus the disk-hole, the topological degeneracy associated with it is just $\dim(g; A_1, \dots, A_{N_p}, \bar{X})$. In other words, the excitation through the removed disk is just like a plaquette excitation, although we allow its quantum number to take any value $X \in \mathcal{Z}(\mathcal{C})$ rather than forcing it to always be a fluxon. Furthermore, since we intend to sew this object on to other similar objects such that the disk-hole is patched up, we do not include any internal degeneracy for the hole. Indeed, as explained in Ref. [38], these internal degeneracies are only relevant for open strings.

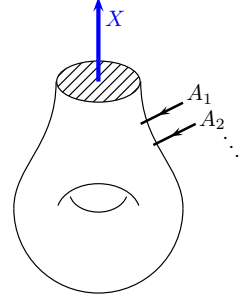


FIG. 2. A genus g surface with a disk (shaded) removed. Here, we have drawn $g = 1$ and we have allowed a quantum number $X \in \mathcal{Z}(\mathcal{C})$ to be coming out of the hole. In addition, we have shown that fluxons $A_p \in \mathcal{F}$ are penetrating the plaquettes on the surface.

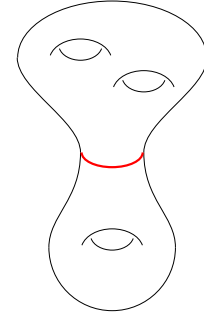


FIG. 3. Sewing together two objects as in Fig. 2. Here, we have sewn together genus $g_R = 1$ (lower half) with $g_{\bar{R}} = 2$ (upper half), connected at the red line, to obtain an object with genus $g = g_R + g_{\bar{R}} = 3$. We say that the red line here goes around a *throat* separating $g_R = 1$ from $g_{\bar{R}} = 2$.

Using Eqs. (7)-(9), one then gets

$$\dim(g; A_1, \dots, A_{N_p}, \bar{X}) = \sum_{C \in \mathcal{Z}(\mathcal{C})} \left[\prod_{p=1}^{N_p} S_{A_p, C} \right] \times S_{\bar{X}, C}^{2-2g-(N_p+1)}. \quad (10)$$

Importantly, for $g = 0$, $\dim(g; A_1, \dots, A_{N_p}, \bar{X})$ vanishes unless X can be obtained by the fusion of multiple fluxons. We write $X \in \mathcal{F}^\otimes$, where \mathcal{F}^\otimes denotes the subset of simple objects of $\mathcal{Z}(\mathcal{C})$ that can be obtained by fusion of fluxons (i.e., elements of \mathcal{F}). Hence, one has:

$$\mathcal{F} \subseteq \mathcal{F}^\otimes \subseteq \mathcal{Z}(\mathcal{C}), \quad (11)$$

Similarly, for $g = 1$, we need to have $X \in (\mathcal{F}^\otimes \times (B_1 \times \bar{B}_1))$ for some object $B_1 \in \mathcal{Z}(\mathcal{C})$ around the handle, and so forth. More generally, $\dim(g; A_1, \dots, A_{N_p}, \bar{X})$ vanishes if $X \notin \mathcal{F}^\otimes \times \mathcal{G}^{\otimes g}$, where \mathcal{G} is the set of objects in the fusion products $B \times \bar{B}$, for all $B \in \mathcal{Z}(\mathcal{C})$, and $\mathcal{G}^{\otimes g}$ means the set of objects generated by fusing g objects in \mathcal{G} together.

These effective dimensions are arranged so that we can sew together two of these surfaces at their holes to obtain

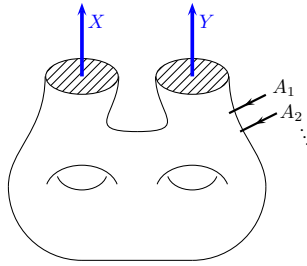


FIG. 4. A genus- g surface with two disks (shaded) removed. Here, we have drawn $g = 2$ and we have allowed a quantum numbers $X, Y \in \mathcal{Z}(\mathcal{C})$ to be coming out of the holes. In addition we have shown that fluxons $A_j \in \mathcal{F}$ are penetrating the plaquettes on the surface.

the degeneracy of a surface with no holes, as shown in Fig. 3. The procedure of cutting disk holes in surfaces and reconnecting them in this way is known as taking the “connected sum” of surfaces. In particular, we want to assemble together such an object \mathcal{R} of genus $g_{\mathcal{R}}$ with $N_p^{\mathcal{R}}$ plaquettes having fluxes $A_1, \dots, A_{N_p^{\mathcal{R}}}$ and a flux X coming out of the hole, together with an object $\bar{\mathcal{R}}$ of genus $g_{\bar{\mathcal{R}}}$ with $N_p^{\bar{\mathcal{R}}}$ plaquettes having fluxes $A_{N_p^{\mathcal{R}}+1}, \dots, A_{N_p}$ with flux X going into the hole (\bar{X} coming out of the hole). The resulting object $\mathcal{R} \cup \bar{\mathcal{R}}$ genus $g = g_{\mathcal{R}} + g_{\bar{\mathcal{R}}}$ surface, as shown in Fig. 3, then has a total effective dimension [making use of the property of Eq. (6)]

$$\begin{aligned} \dim(g; A_1, \dots, A_{N_p}) &= \sum_{X \in \mathcal{Z}(\mathcal{C})} \dim(g_{\mathcal{R}}; A_1, \dots, A_{N_p^{\mathcal{R}}}, \bar{X}) \\ &\quad \dim(g_{\bar{\mathcal{R}}}; A_{N_p^{\mathcal{R}}+1}, \dots, A_{N_p}, X). \end{aligned} \quad (12)$$

Similarly, we can write a degeneracy for a genus- g surface with two disks removed having quantum numbers X and Y coming out of the missing disk-holes, as shown in Fig. 4. Using Eqs. (7)-(9), the topological degeneracy of this object can be written as:

$$\begin{aligned} \dim(g; A_1, \dots, A_{N_p}, \bar{X}, \bar{Y}) &= \sum_{C \in \mathcal{Z}(\mathcal{C})} \left[\prod_{p=1}^{N_p} S_{A_p, C} \right] \times \\ &\quad S_{\bar{X}, C} S_{\bar{Y}, C} S_{1, C}^{2-2g-(N_p+2)}. \end{aligned} \quad (13)$$

Again, we have not included the internal degeneracy associated with the quantum number in the hole, since we intend to sew these holes together. Setting $\bar{Y} = X$ in Eq. (13), we obtain the effective degeneracy for a surface with an additional handle, and a particular flux X through that handle (see Fig. 5). For example, a sphere with two holes cut is a cylinder. If we connect these two holes to each other, we get a torus. More generally, if we cut two holes in a genus- g object with plaquette fluxes A_1, \dots, A_{N_p} and reconnect the two holes together we get a genus $(g+1)$ -object. The full topological degeneracy of

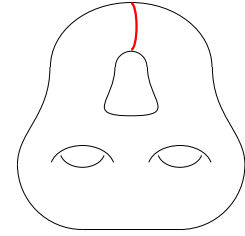


FIG. 5. Sewing together the two open faces of Fig. 4. The object in Fig. 4 is genus $g = 2$, but when we sew together the two holes (which is only possible if $Y = \bar{X}$), we have an object of genus $g = 3$. The red line here goes around a *handle*.

such an object (with unrestricted flux through the handle) is then

$$\begin{aligned} \dim(g+1; A_1, \dots, A_{N_p}) &= \sum_{X \in \mathcal{Z}(\mathcal{C})} \\ \dim(g; A_1, \dots, A_{N_p}, \bar{X}, X). \end{aligned} \quad (14)$$

An example of this type of sewing is shown in Fig. 5.

IV. PARTITION FUNCTIONS

A. Results for the RSN model

Once the degeneracies of the energy levels are determined, it is pretty easy to compute the finite-temperature partition function of the RSN model (2). For a genus- g surface with N_p plaquettes, it is given by

$$\begin{aligned} Z(g, N_p) &= \text{Tr}(e^{-\beta H}) \\ &= \sum_{A_1, \dots, A_{N_p} \in \mathcal{F}} \dim(g; A_1, \dots, A_{N_p}) \\ &\quad \sum_{a_1=1}^{n_{A_1,1}} \sum_{a_2=1}^{n_{A_2,1}} \dots \sum_{a_{N_p}=1}^{n_{A_{N_p},1}} e^{\beta \sum_{p=1}^{N_p} J_p^{A_p, a_p}}, \end{aligned} \quad (15)$$

where $\beta = 1/T$, is the inverse temperature (we set $k_B = 1$), and where the energy associated with a fixed fluxon configuration of $\{A_1, A_2, \dots, A_{N_p}\}$, with multiplicity indices $\{a_1, a_2, \dots, a_{N_p}\}$ is given by Eq. (3). Using Eq. (9), and the fact that S is a symmetric and unitary matrix, one can rewrite this partition function in the following simple form:

$$Z(g, N_p) = \sum_{C \in \mathcal{Z}(\mathcal{C})} S_{1,C}^{2-2g} \prod_{p=1}^{N_p} z_{p,C}, \quad (16)$$

where we introduced

$$z_{p,C} = \sum_{A \in \mathcal{F}} \sum_{a=1}^{n_{A,1}} \frac{S_{A,C}}{S_{1,C}} e^{\beta J_p^{A,a}}. \quad (17)$$

It is interesting to analyze the global structure of Eq. (16), which is one of the main results of our paper. Indeed, this partition function is written as a sum of terms which are simple products over all plaquettes. This is reminiscent of the fact that the Hamiltonian is a sum of local commuting projectors together with some nonlocal constraints given by the topological degeneracies.

Interestingly, in the thermodynamic limit, the sum in Eq. (16) is dominated by a special set of objects C which maximizes the ratio $S_{A,C}/S_{1,C}$. As explained in Appendix A, for $A \in \mathcal{F}$, this quantity is maximized if C belongs to the pure fluxon set $\mathcal{P} \subseteq \mathcal{F}$. A pure fluxon C is a fluxon which obeys $n_{C,1} = d_C$. On the one hand, according to Eq. (A11), for any A and $C \in \mathcal{Z}(\mathcal{C})$, we have

$$|S_{A,C}| \leq d_A d_C / \mathcal{D}, \quad (18)$$

where d_A is the quantum dimension of the particle A and

$$\mathcal{D} = \sqrt{\sum_{C \in \mathcal{Z}(\mathcal{C})} d_C^2}, \quad (19)$$

is the total quantum dimension of $\mathcal{Z}(\mathcal{C})$. On the other hand, if $A \in \mathcal{F}$ and $C \in \mathcal{P}$ (or the contrary), the inequality (18) becomes an equality $S_{A,C} = d_A d_C / \mathcal{D}$. In other words, *pure fluxons braid trivially with all fluxons*. Hence, when C is a pure fluxon, one has

$$z_{p,C} = \sum_{A \in \mathcal{F}} \sum_{a=1}^{n_{A,1}} d_A e^{\beta J_p^{A,a}} \equiv z_p, \quad (20)$$

is independent of C . For any $T > 0$, we therefore get

$$Z(g, N_p) \underset{N_p \rightarrow \infty}{\simeq} M_g \mathcal{D}^{2g-2} \prod_{p=1}^{N_p} z_p, \quad (21)$$

where we introduced

$$M_g \equiv \sum_{A \in \mathcal{P}} n_{A,1}^{2-2g} = \sum_{A \in \mathcal{P}} d_A^{2-2g}. \quad (22)$$

For a commutative input category, M_g is simply the number of pure fluxons as $n_{A,1} = 1$ for $A \in \mathcal{F}$, i.e., $M_g = |\mathcal{P}|$, for any genus. It also corresponds to the number of Abelian fluxons.

B. Infinite-temperature limit and Hilbert-space dimension

The Hilbert space dimension can be easily computed by taking the infinite-temperature limit of the partition function Eq. (16). In this limit, using the fluxon identity

$$S \mathbf{n}_1 = \mathbf{n}_1, \quad (23)$$

where \mathbf{n}_1 is the vector with components $n_{C,1}$ ($n_{C,1} = 0$, if $C \notin \mathcal{F}$) [38], one gets

$$\lim_{T \rightarrow \infty} z_{p,C} = \frac{n_{C,1}}{S_{1,C}}. \quad (24)$$

Then, one straightforwardly obtains:

$$\begin{aligned} \dim \mathcal{H} &= \lim_{T \rightarrow \infty} Z(g, N_p), \\ &= \sum_{C \in \mathcal{Z}(\mathcal{C})} S_{1,C}^{2-2g} \left(\frac{n_{C,1}}{S_{1,C}} \right)^{N_p}, \\ &= \sum_{C \in \mathcal{F}} S_{1,C}^{-N_v/2} n_{C,1}^{N_p}. \end{aligned} \quad (25)$$

For commutative input \mathcal{C} , this result is in agreement with the one given in Ref. [39]. We also used the fact that, for a trivalent graph, the Euler-Poincaré characteristic gives

$$2 - 2g - N_p = -N_v/2, \quad (26)$$

where N_v is the number of vertices.

In the limit of large N_p , we have

$$\dim \mathcal{H} \underset{N_p \rightarrow \infty}{\simeq} M_g \mathcal{D}^{N_v/2}, \quad (27)$$

which show that the Hilbert space is not a tensor product of local Hilbert spaces.

C. Cutting and gluing partition functions

Using our results on effective degeneracies of Sec. III C, we can also write effective partition functions for surfaces with holes cut in them. Note that we are not including any energy associated with the flux through the hole. For a genus- g surface with a single hole carrying a flux $X \in \mathcal{Z}(\mathcal{C})$ (see Fig. 2 for $g = 1$) and N_p plaquettes, the (effective) partition function can be computed using Eq. (10) and reads:

$$Z_X(g, N_p) = \sum_{C \in \mathcal{Z}(\mathcal{C})} S_{\bar{X},C} S_{1,C}^{1-2g} \prod_{p=1}^{N_p} z_{p,C}. \quad (28)$$

where $z_{p,C}$ is given in Eq. (17).

Analogous to what is done in Eq. (12), we can compute the partition function of a surface obtained by gluing together one object of genus g_R with N_p^R plaquettes with another object of genus $g_{\bar{R}}$ with $N_p^{\bar{R}}$ plaquettes

$$Z(g_R + g_{\bar{R}}, N_p^R + N_p^{\bar{R}}) = \sum_{X \in \mathcal{Z}(\mathcal{C})} Z_X(g_R, N_p^R) Z_{\bar{X}}(g_{\bar{R}}, N_p^{\bar{R}}). \quad (29)$$

This is precisely the sewing operation depicted in Fig. 3.

Similarly, we can write an effective partition function associated to a surface with two holes in it (see Fig. 4). Again, using Eq. (13), this expression can be written as

$$Z_{X,Y}(g, N_p) = \sum_{C \in \mathcal{Z}(\mathcal{C})} S_{\bar{X},C} S_{\bar{Y},C} S_{1,C}^{-2g} \prod_{p=1}^{N_p} z_{p,C}. \quad (30)$$

These holes can then be glued to each other in order to increase the genus, as in Eq. (14), to give

$$Z(g+1, N_p) = \sum_{X \in \mathcal{Z}(\mathcal{C})} Z_{X, \bar{X}}(g, N_p), \quad (31)$$

which is the sewing depicted in Fig. 5.

The three partition functions Z , Z_X , and $Z_{X,Y}$ will be used in Sec. VI to compute the thermal averages of some operators.

V. THERMODYNAMICS FOR THE SN MODEL

The simple form of the general partition function given in Eq. (16) allows one to study several quantities. Here, we shall discuss them for the SN model for which $J_p^{A,a} = \delta_{A,1}$, for all p 's. In this case and keeping in mind that $d_1 = n_{1,1} = 1$, Eqs. (17)-(23) lead to

$$z_{p,C} = \frac{n_{C,1}}{S_{1,C}} - 1 + e^\beta, \quad (32)$$

which is independent of p . This result is particularly pleasing since it depends only on the internal multiplicities $n_{C,1}$ and on $S_{1,C} = d_C/\mathcal{D}$.

A. Partition functions in the thermodynamic limit

As explained in Sec. IV A, in the large- N_p limit, the sum in Eq.(16) is dominated by pure fluxons ($n_{C,1} = d_C$) so that, for the SN model, one has:

$$Z(g, N_p) \underset{N_p \rightarrow \infty}{\simeq} (\mathcal{D} - 1 + e^\beta)^{N_p} \sum_{C \in \mathcal{P}} S_{1,C}^{2-2g}, \quad (33)$$

where we used the identity $S_{1,C} = d_C/\mathcal{D}$, for all C . A similar result was obtained for the case of the Fibonacci input category by [44]. Here, we obtain it for any input UFC.

Similarly, one has:

$$Z_X(g, N_p) \underset{N_p \rightarrow \infty}{\simeq} (\mathcal{D} - 1 + e^\beta)^{N_p} \sum_{C \in \mathcal{P}} S_{\bar{X},C} S_{1,C}^{1-2g}, \quad (34)$$

and

$$Z_{X,Y}(g, N_p) \underset{N_p \rightarrow \infty}{\simeq} (\mathcal{D} - 1 + e^\beta)^{N_p} \sum_{C \in \mathcal{P}} S_{\bar{X},C} S_{\bar{Y},C} S_{1,C}^{-2g}. \quad (35)$$

B. Ground-state degeneracy

The zero- T limit of the partition function Z allows one to compute straightforwardly the ground-state degeneracy of the SN Hamiltonian (1). This topology-dependent

degeneracy is given by:

$$\lim_{T \rightarrow 0} Z e^{\beta E_0} = \sum_{C \in \mathcal{Z}(\mathcal{C})} S_{1,C}^{2-2g}, \quad (36)$$

where $E_0 = -N_p$, is the ground-state energy. This result is exactly the TQFT result [43] for the degeneracy on a surface of genus g that can also be obtained directly from Eq. (9) by imposing the no-flux condition, $A_p = \mathbf{1}$, for all p 's, which defines the ground-state manifold of the SN model.

C. Energy, specific heat, and entropy

Using Eqs. (16) and (32), it is straightforward to compute several thermodynamical quantities for the SN model. Here, we discuss some of them by considering directly the thermodynamic limit (33) for which expression becomes especially simple.

In the large- N_p limit, the energy per plaquette is given by

$$e = \lim_{N_p \rightarrow \infty} -\frac{1}{N_p} \frac{\partial \ln Z}{\partial \beta} = -\frac{e^\beta}{\mathcal{D} - 1 + e^\beta}. \quad (37)$$

We will see in Sec. VID how to obtain this result from the projectors directly [see Eq. (52)].

Similarly, the specific heat per plaquette is given by

$$c = \lim_{N_p \rightarrow \infty} \frac{\beta^2}{N_p} \frac{\partial^2 \ln Z}{\partial \beta^2} = \frac{e^\beta \beta^2 (\mathcal{D} - 1)}{(\mathcal{D} - 1 + e^\beta)^2}. \quad (38)$$

These expressions which hold for any UFC are exactly the same as the one derived in Ref. [39] where only modular input UFCs were considered. This very simple form of the specific heat shows that, c is always a smooth function of the temperature, indicating the *absence of finite-temperature phase transition in this model*. This latter result also holds for the RSN model and is in agreement with the general result derived by Hastings [25] which holds for any local commuting projector Hamiltonian in two dimensions.

Finally, the entropy is:

$$S = -\beta \frac{\partial \ln Z}{\partial \beta} + \ln Z. \quad (39)$$

Using Eq. (33), one gets in the thermodynamic limit at $T > 0$

$$S \underset{N_p \rightarrow \infty}{\simeq} N_p \left[\ln(\mathcal{D} - 1 + e^\beta) - \frac{\beta e^\beta}{\mathcal{D} - 1 + e^\beta} \right] + \ln \frac{M_g}{\mathcal{D}^{2-2g}}, \quad (40)$$

where M_g is given in Eq. (22). This consists of a volume (extensive) term and a constant term. In the infinite-temperature limit, this expression simply becomes

$$\lim_{T \rightarrow \infty} S = \ln(\dim \mathcal{H}) \underset{N_p \rightarrow \infty}{\simeq} \frac{N_v}{2} \ln \mathcal{D} + \ln M_g. \quad (41)$$

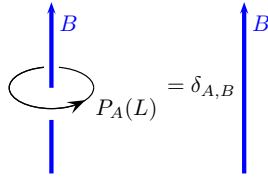


FIG. 6. Schematic representation of a projector P_A measuring a particle B . The loop L goes counterclockwise around the region being projected.

For future reference, we note that the constant term, $\ln M_g$, is not related to quantum entanglement but to the fact that the Hilbert space is constrained by the fusion rules (vertex defects are forbidden).

VI. THERMAL AVERAGE OF PROJECTORS

Having established the basic thermodynamics, we turn to calculate the thermal expectation of certain operators of interest. The first operators we will study are the topological projection operators $P_X(L)$ for $X \in \mathcal{Z}(\mathcal{C})$ and L a closed path on our surface. Following the same line as in Sec. III C, we will keep in mind that L is a closed contour separating two regions \mathcal{R} and $\bar{\mathcal{R}}$.

As a complete set of orthogonal projection operators, these satisfy

$$P_X(L)P_Y(L) = \delta_{X,Y}P_X(L), \quad (42)$$

and

$$\sum_{X \in \mathcal{Z}(\mathcal{C})} P_X(L) = \mathbb{1}, \quad (43)$$

where the sum is over all objects of the Drinfeld center $\mathcal{Z}(\mathcal{C})$. Physically, $P_X(L)$ projects to a configuration where the flux through the loop L is given by the particle type $X \in \mathcal{Z}(\mathcal{C})$. For definiteness, we define the direction of the loop L such that it travels counterclockwise around the region of interest. This projection is shown graphically in Fig. 6. The expectation of these operators will be obtained using our cutting and gluing rules from Sec. IV C. We consider here three different types of loops. Firstly, we discuss loops around a *handle* L_h , (see red line in Fig. 5), and secondly loops around a *throat* L_t (see red line in Fig. 3). The case of a *contractible* loop L_c is finally discussed as a special case of throat. The main results of this section are given in Eqs. (44), (48), and (49).

Remarkably, these expressions are exact for any temperature, any system size, any trivalent graph, any choice of the couplings, and any input UFC.

A. Topological expectations

Depending on the couplings $J_p^{A,a}$'s, the ground state of the Hamiltonian (2) may or may not have nontrivial

fluxons through plaquettes. At zero temperature, our projectors will measure the topological quantum numbers [i.e. $X \in \mathcal{Z}(\mathcal{C})$] through these loops — which are fixed by the nature of the ground state.

At any finite temperature, there is a nonzero probability that each of the plaquettes will not be in their ground state. These excitations carry topological quantum numbers, and we should expect that, for a sufficiently large system, the topological properties of the system will be scrambled. For example, a loop encircling a large enough region will surround a completely unknown topological quantum number. However, not all topological information will be erased at finite temperature at long distances. Since we have enforced the vertex constraint at the level of the Hilbert space (rather than as a term in the Hamiltonian as was originally done in Ref. [14]), we have forbidden certain types of defects, and topological information associated to them can remain at any temperature.

B. Handles

To implement a projector on a loop L_h around a handle of a genus- g surface with N_p plaquettes, we refer back to Eq. (31). This representation of the partition function of the full system is already written in terms of a sum of effective partition function $Z_{X,\bar{X}}$ where a flux X is imposed in the chosen handle after gluing. Thus, the thermal average of the operator that projects to have flux X through the chosen handle is simply given by

$$\langle P_X(L_h) \rangle = \frac{Z_{X,\bar{X}}(g-1, N_p)}{Z(g, N_p)}, \quad (44)$$

where Z and $Z_{X,\bar{X}}$ are given for arbitrary couplings in Eq. (16) and Eq. (30), respectively. This quantity, which only depends on β , g and N_p , vanishes if $X \notin \mathcal{F}^\otimes \times \mathcal{G}^\otimes$ [see discussion after Eq. (11)]. Using Eq. (31), one can easily check the identity (43).

As done for the partition functions, it is interesting to study the behavior of $\langle P_X(L_h) \rangle$ in some limiting cases. Let us first discuss the large- N_p limit at *any* nonzero temperature. In this limit, as explained in Sec. IV A, the sums over all objects of the Drinfeld centers appearing in Eq. (44) are dominated by the pure fluxons, and $z_{p,C}$ becomes independent of C [see Eq. (20)]. Hence, one simply obtains:

$$\lim_{N_p \rightarrow \infty} \langle P_X(L_h) \rangle = \frac{\sum_{C \in \mathcal{P}} S_{X,C} S_{\bar{X},C} S_{1,C}^{2-2g}}{\sum_{C \in \mathcal{P}} S_{1,C}^{2-2g}}. \quad (45)$$

Again, unitarity of the symmetric S -matrix ensures the relation (43). The result of Eq. (45) is independent of the couplings and of the temperature, as long as $T > 0$.

One can also easily get the behavior of $\langle P_X(L_h) \rangle$ in the infinite-temperature limit. In this limit, using Eq. (24),

Eq. (44) becomes

$$\lim_{T \rightarrow \infty} \langle P_X(L_h) \rangle = \frac{\sum_{C \in \mathcal{Z}(\mathcal{C})} S_{X,C} S_{\bar{X},C} S_{\mathbf{1},C}^{2-2g-N_p} n_{C,1}^{N_p}}{\sum_{C \in \mathcal{Z}(\mathcal{C})} S_{\mathbf{1},C}^{2-2g-N_p} n_{C,1}^{N_p}}, \quad (46)$$

which is nontrivial because we are considering a restricted Hilbert space (no violation of the vertex constraints). Remarkably, this result is also independent of the couplings $J_p^{A,a}$.

Finally, as for the zero- T partition function, $\langle P_X(L_h) \rangle$ depends on the couplings. For the SN model, one gets

$$\lim_{T \rightarrow 0} \langle P_X(L_h) \rangle = \frac{\sum_{C \in \mathcal{Z}(\mathcal{C})} S_{X,C} S_{\bar{X},C} S_{\mathbf{1},C}^{2-2g}}{\sum_{C \in \mathcal{Z}(\mathcal{C})} S_{\mathbf{1},C}^{2-2g}}, \quad (47)$$

which is valid for any value of N_p . This result differs from Eq. (45) in that the sum is over all objects of the Drinfeld center $\mathcal{Z}(\mathcal{C})$ rather than just the subset of pure fluxons \mathcal{P} .

C. Throats

Let us now discuss the case where the loop is defined around a throat, i.e., a loop L_t around a contour separating genus $g_{\mathcal{R}}$ and $g_{\bar{\mathcal{R}}}$ surfaces such as the red line shown in Fig. 3. To compute $\langle P_X(L_t) \rangle$, we follow roughly the same strategy, writing the genus- $g = g_{\mathcal{R}} + g_{\bar{\mathcal{R}}}$ partition function in terms of partition functions of the two pieces as in Eq. (29). Fixing the value of the flux though the throat to X gives us

$$\langle P_X(L_t) \rangle = \frac{Z_X(g_{\mathcal{R}}, N_p^{\mathcal{R}}) Z_{\bar{X}}(g_{\bar{\mathcal{R}}}, N_p^{\bar{\mathcal{R}}})}{Z(g, N_p)}, \quad (48)$$

where $N_p = N_p^{\mathcal{R}} + N_p^{\bar{\mathcal{R}}}$ is the total number of plaquettes. Again, one can easily check the identity (43) using Eq. (29).

As done for $\langle P_X(L_h) \rangle$, it is straightforward to extract various limiting cases (such as large $N_p^{\mathcal{R}}$, large $N_p^{\bar{\mathcal{R}}}$, or infinite-temperature limits) using Eqs. (20) and (24).

D. Contractible loops

To conclude this section, we consider the case of contractible loops L_c . As one can observe in Fig. 3, if $g_{\mathcal{R}} = 0$ or $g_{\bar{\mathcal{R}}} = 0$, the red line becomes contractible. Thus, $\langle P_X(L_c) \rangle$ can be directly computed from Eq. (48) by setting one of the genuses, let's say $g_{\bar{\mathcal{R}}}$, to 0. We then have

$$\langle P_X(L_c) \rangle = \frac{Z_X(g_{\mathcal{R}}, N_p^{\mathcal{R}}) Z_{\bar{X}}(0, N_p^{\bar{\mathcal{R}}})}{Z(g, N_p)}, \quad (49)$$

where the contractible side has $N_p^{\bar{\mathcal{R}}}$ plaquettes, while the other side has genus $g_{\mathcal{R}}$ and $N_p^{\mathcal{R}}$ plaquettes, and the full system has genus $g = g_{\mathcal{R}}$ and $N_p = N_p^{\mathcal{R}} + N_p^{\bar{\mathcal{R}}}$ plaquettes. Because $g_{\bar{\mathcal{R}}} = 0$, this expectation value must be zero unless $X \in \mathcal{F}^{\otimes}$ [see also the comment just after Eq. (10)]. That is, X must be obtainable by the fusion of multiple fluxons.

For the special case of the SN model, Eq. (49) becomes very simple. For instance, in the zero- T limit, one can check that

$$\lim_{T \rightarrow 0} \langle P_X(L_c) \rangle = \delta_{X,1}, \quad (50)$$

which simply indicates that, for all ground states of the SN model, there is no nontrivial fluxon in any contractible loop. Noncontractible loops may however contain nontrivial fluxes [see, e.g., Eq. (47) for handles].

In the limit where the side with genus $g_{\mathcal{R}}$ is large ($N_p^{\mathcal{R}} \gg 1$) using Eqs. (32), (33), and (34), one gets:

$$\lim_{N_p^{\mathcal{R}} \rightarrow \infty} \langle P_X(L_c) \rangle = d_X \sum_{C \in \mathcal{Z}(\mathcal{C})} S_{\bar{X},C} S_{\mathbf{1},C} \times \left(\frac{\mathcal{D}^{\frac{n_{C,1}}{d_C}} - 1 + e^{\beta}}{\mathcal{D} - 1 + e^{\beta}} \right)^{N_p^{\mathcal{R}}}, \quad (51)$$

if $X \in \mathcal{F}^{\otimes}$, and 0 otherwise.

In the special case where $X = \mathbf{1}$ and $N_p^{\mathcal{R}} = 1$, the projection operator $P_{\mathbf{1}}(L_c)$ is exactly the plaquette projector B_p used to define the Hamiltonian in Eq. (2) provided L_c is the loop encircling (only) the plaquette p .

In the case of a single plaquette, $\langle P_X(L_c) \rangle \neq 0$ iff $X \in \mathcal{F}$. Using the fact that S is unitary and symmetric as well as Eq. (23), one finds:

$$\lim_{N_p^{\mathcal{R}} \rightarrow \infty} \langle P_{\mathbf{1}}(L_c) \rangle = \frac{e^{\beta}}{\mathcal{D} - 1 + e^{\beta}} = -e, \quad (52)$$

where e is given in Eq. (37) when $X = \mathbf{1}$, and

$$\lim_{N_p^{\mathcal{R}} \rightarrow \infty} \langle P_X(L_c) \rangle = \frac{d_X n_{X,1}}{\mathcal{D} - 1 + e^{\beta}}, \quad (53)$$

when $X \in \mathcal{F}^*$, i.e., is a nontrivial fluxon. This thermal average of a nontrivial fluxon projector has been computed in Ref. [44] in the Fibonacci SN model and used to discuss an effective Pauli exclusion principle (see also Ref. [39]).

VII. WEGNER-WILSON LOOPS

A. From projectors to WWL

Wegner-Wilson loops (WWL) are a different type of string operator, which should be thought of as quasiparticle world lines. These are closely related to the projection operators $P_A(L)$ discussed in the previous section.

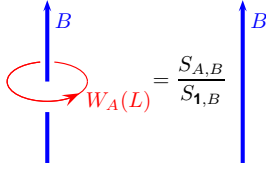


FIG. 7. A Wegner-Wilson loop operator W_A acting on a string B . This is known as the “unlinking” relation.

For any given closed loop L on our surface, the unlinking relation (see, e.g., Refs. [45, 46]) shown in Fig. 7 directly gives:

$$W_A(L) = \sum_{B \in \mathcal{Z}(\mathcal{C})} \frac{S_{A,B}}{S_{1,B}} P_B(L). \quad (54)$$

Using the unitarity of S , one also gets the inverse transformation

$$P_A(L) = S_{1,A} \sum_{B \in \mathcal{Z}(\mathcal{C})} S_{A,B}^* W_B(L). \quad (55)$$

Using Eqs. (43) and (54), it is easy to show that W_1 is actually the identity operator $\mathbf{1}$.

The closed string operators W_A satisfy the fusion algebra

$$W_A(L) W_B(L) = \sum_{C \in \mathcal{Z}(\mathcal{C})} N_{A,B}^C W_C(L), \quad (56)$$

where $N_{A,B}^C$ are the fusion multiplicity coefficients of $\mathcal{Z}(\mathcal{C})$. Equation (56) can be proven by using the Verlinde formula (8) along with the unitarity of S and the projector property of $P_A(L)$ given in Eq. (42).

A remarkable case of Eq. (55) is obtained for the projector onto the vacuum $A = \mathbf{1}$ for which

$$P_{\mathbf{1}}(L) = \sum_{B \in \mathcal{Z}(\mathcal{C})} \frac{d_B}{\mathcal{D}^2} W_B(L). \quad (57)$$

A slightly different normalization of this object,

$$\Omega(L) = \mathcal{D} P_{\mathbf{1}}(L), \quad (58)$$

is known as a Kirby strand [46], and is used extensively in Appendix C. As explained in Sec. VID, if L surrounds a single plaquette p , then $P_{\mathbf{1}}(L) = B_p$.

Using the results obtained in Sec. VI for the projectors, it is straightforward to obtain the thermal average of WWL operators using (54). For instance, for a large genus- g surface, at any nonzero temperature, and for arbitrary couplings, one gets from Eqs. (45) and (54)

$$\lim_{N_p \rightarrow \infty} \langle W_A(L_h) \rangle = \frac{\sum_{C \in \mathcal{P}} N_{AC}^C S_{1,C}^{2-2g}}{\sum_{C \in \mathcal{P}} S_{1,C}^{2-2g}}, \quad (59)$$

where we used the Verlinde formula (8). Such a WWL around a handle was studied, for example, in Ref. [47] in

a similar context. It shows a different behavior at zero temperature:

$$\lim_{T \rightarrow 0} \langle W_A(L_h) \rangle = \frac{\sum_{C \in \mathcal{Z}(\mathcal{C})} N_{AC}^C S_{1,C}^{2-2g}}{\sum_{C \in \mathcal{Z}(\mathcal{C})} S_{1,C}^{2-2g}}, \quad (60)$$

where we used Eqs. (47) and (54). Note how the Drinfeld center replaces the set of pure fluxons in the above sums when contrasting the $T = 0$ and $T > 0$ behaviors.

For the simple case of the SN model, one recovers the obvious fact that, at zero temperature, for any $A \in \mathcal{Z}(\mathcal{C})$, and for any contractible loop L_c ,

$$\lim_{T \rightarrow 0} \langle W_A(L_c) \rangle = d_A. \quad (61)$$

Indeed, for any ground state of the SN model, one has only the vacuum in each plaquette. Thus, this result can be directly obtained from the unlinking relation (see Fig. 7 for $B = \mathbf{1}$). One can also obtain a simple expression of the WWL operators in the SN model at finite temperature, in the thermodynamic limit. Using Eq. (51) and (54) one gets:

$$\lim_{N_p^{\mathcal{R}} \rightarrow \infty} \langle W_A(L_c) \rangle = d_A \left(\frac{\mathcal{D}^{\frac{n_{A,1}}{d_A}} - 1 + e^\beta}{\mathcal{D} - 1 + e^\beta} \right)^{N_p^{\mathcal{R}}}. \quad (62)$$

B. Confinement

The behavior of $\langle W_A(L) \rangle$ when the size of the region \mathcal{R} encircled by the loop L varies can be used to diagnose the confinement/deconfinement properties of the quasiparticle A (see, e.g., Ref. [48] for a study of the WWL operators in the SN model perturbed by a string tension [49, 50]). Typically, in the case of a contractible loop L_c , a deconfined quasiparticle A corresponds to a “perimeter law”, i.e., the WWL decays exponentially with the perimeter $|L_c|$ of the loop L_c

$$\langle W_A(L_c) \rangle \sim e^{-c_1 |L_c|}, \quad (63)$$

when L_c grows and where $c_1 > 0$. In the extreme case where $c_1 = 0$ (no decay of the WWL), it is known as the “zero law” [51].

A confined quasiparticle A corresponds to an “area law”, i.e., the WWL decays exponentially with the area \mathcal{A} of the region delimited by L_c (i.e., \mathcal{R} or \mathcal{R} since we are on a closed surface)

$$\langle W_A(L_c) \rangle \sim e^{-c_2 \mathcal{A}}, \quad (64)$$

when L_c grows and where $c_2 > 0$.

Let us analyze the confining properties of the quasiparticles in the special case of the SN model. As can already be seen in Eq. (61), at zero temperature, $W_A(L_c)$ obeys a zero law (see Ref. [48] for further discussions). This means that all quasiparticles are deconfined in the ground state, which is a fingerprint of a topologically

ordered phase. By contrast, at any finite temperature, Eq. (62) indicates an area law, i.e., a confinement, for all particles of the Drinfeld center except for pure fluxons identified by $n_{A,1} = d_A$. Indeed, for pure fluxons, one always has

$$\langle W_A(L_c) \rangle = d_A, \quad (65)$$

indicating a deconfinement of these particles at any temperature. Equation (65) suggests that pure fluxons are insensitive to the presence of other fluxons in the system, i.e., that they braid trivially with all fluxons. This trivial braiding property, already mentioned in Sec. IV A, can be summarized as follows: *if A is a pure fluxon, i.e., if $n_{A,1} = d_A$, then one has $S_{A,B} = d_A d_B / D$, for any fluxon.* As a byproduct, this property also holds for any particle $B \in \mathcal{F}^\otimes$. For all other particles $A \notin \mathcal{F}$, one has $n_{A,1} < d_A$, and Eq. (62) describes an area law. More generally, one may write

$$\langle W_A(L_c) \rangle = d_A e^{-N_p^{\mathcal{R}}/N_A^*}, \quad (66)$$

where we introduced the temperature-dependent characteristic area

$$N_A^* = \left[\ln \left(\frac{D - 1 + e^\beta}{D^{\frac{n_{A,1}}{d_A}} - 1 + e^\beta} \right) \right]^{-1}, \quad (67)$$

which diverges for $A \in \mathcal{P}$ ($n_{A,1} = d_A$) and is minimum for $A \notin \mathcal{F}$ ($n_{A,1} = 0$). In other words, particles that are not fluxons are strongly confined.

VIII. TOPOLOGICAL MUTUAL INFORMATION

One way to characterize topological order at zero temperature is to compute the topological entanglement entropy introduced in Refs. [52, 53] (see also Ref. [54]). However, at finite temperature, this quantity, defined as the constant term of the von Neumann entanglement entropy, suffers from several problems which have led Iblisdir *et al.* to rather consider the topological mutual information I_{topo} [55, 56]. The main issue is that the finite-temperature entanglement entropy no longer follows an area law but also features an extensive term. It is therefore no longer symmetric between the inner and outer region of the contour, and cannot be thought of as measuring only the entanglement between these regions.

A. Definitions and conjecture

For a bipartition of the system into two regions \mathcal{R} and $\bar{\mathcal{R}}$, the mutual information is defined as:

$$I_{\mathcal{R}} = S_{\mathcal{R}} + S_{\bar{\mathcal{R}}} - S_{\mathcal{R} \cup \bar{\mathcal{R}}} = I_{\bar{\mathcal{R}}}, \quad (68)$$

where $S_{\mathcal{R}} = -\text{Tr}_{\mathcal{R}} \rho_{\mathcal{R}} \ln \rho_{\mathcal{R}}$ is the von Neumann entropy, and $\rho_{\mathcal{R}} = \text{Tr}_{\bar{\mathcal{R}}} (e^{-\beta H}) / Z$. In the limit where the length

$|L_c|$ of the boundary L_c between the two regions goes to infinity, one expects the mutual information to behave as [55, 56]

$$I_{\mathcal{R}} = \alpha |L_c| - \gamma. \quad (69)$$

This is often called an “area law” although it implies the perimeter of the loop L_c . The topological mutual information is then defined as $I_{\text{topo}} = -\gamma$. Under some simple assumptions, Iblisdir *et al.* conjectured a general form of I_{topo} at finite temperature for the Kitaev quantum double model [13] based on the Kullback-Leibler divergence [55, 56]. For a surface with $g = 0$, and in the limit where $|L_c| \rightarrow \infty$, Iblisdir *et al.* conjectured that

$$I_{\text{topo}}(T) = - \sum_{A \in \mathcal{Z}(\mathcal{C})} \langle P_A(L_c) \rangle \ln \left[\langle P_A(L_c) \rangle \frac{D^2}{d_A^2} \right], \quad (70)$$

where $P_A(L_c)$ is the projector whose thermal average is given in Eq. (49). As explained in Sec. VID, it is nonvanishing only if $A \in \mathcal{F}^\otimes$.

Although the conjecture (70) has been derived in a different context, it is based on general assumptions [55, 56]. In the following, we will assume that it holds for the SN model on which we focus on. As we shall see, it reproduces the exact results in the zero- T and infinite- T limits. Proving this conjecture for arbitrary temperature is work in progress.

B. Infinite-temperature limit

Generically, one expects zero mutual information at infinite temperature due to a loss of quantum correlations. However, for the SN model, some nontrivial residual information remains in our system because we are working in a restricted Hilbert space (vertex constraint) [57].

The general expression of $\langle P_A(L_c) \rangle$ is given in Eq. (49). Here, for simplicity, we consider the thermodynamic limit where both $N_p^{\mathcal{R}}$ and $N_p^{\bar{\mathcal{R}}}$ go to infinity which, using Eq. (51), yields

$$\lim_{N_p^{\mathcal{R}}, N_p^{\bar{\mathcal{R}}} \rightarrow \infty} \langle P_A(L_c) \rangle = d_A \sum_{C \in \mathcal{P}} S_{\bar{A},C} S_{1,C} = \frac{d_A^2}{D^2} M_0, \quad (71)$$

for $A \in \mathcal{F}^\otimes$, and 0 otherwise [M_0 is defined in Eq. (22)]. This is valid at any finite temperature (but not at $T = 0$). Using Eq. (43), one then obtains

$$I_{\text{topo}}(T = \infty) = -\ln M_0. \quad (72)$$

As mentioned above, this nonvanishing contribution only stems from the fact that, for the model at hand, we work in a restricted Hilbert space. It has no quantum origin, and it does not reflect any long-range entanglement feature of the system. However, it does reflect some topological property, as only vertex configurations resulting from the fusion rules are allowed.

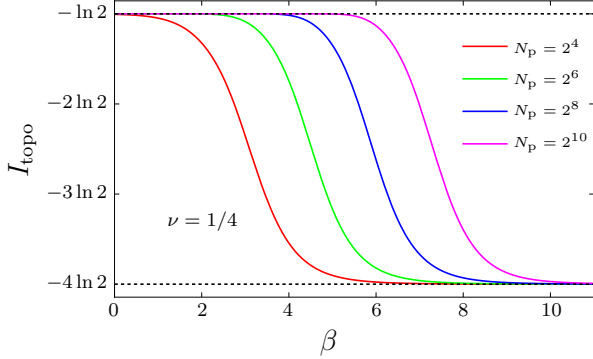


FIG. 8. Topological mutual information of SN model for the Ising category ($\mathcal{D} = 4$, $M_0 = 2$) as a function of $\beta = 1/T$ at fixed $\nu = 1/4$. $I_{\text{topo}}(T=0) = -2 \ln \mathcal{D}$ and $I_{\text{topo}}(T=\infty) = -\ln M_0$ are indicated by dashed lines.

The result (72) is compatible with the one given in Ref. [57] for the topological ‘‘classical’’ entropy. Indeed, at infinite temperature, it was shown in that work, for some special input categories \mathcal{C} , that the topological classical entropy is given by

$$S_{\mathcal{R},\text{topo}}(T=\infty) = -(m_{\overline{\mathcal{R}}} - 1) \ln M, \quad (73)$$

where $m_{\overline{\mathcal{R}}}$ is the number of disconnected pieces in $\overline{\mathcal{R}}$, and where M was identified as the number of Abelian particles in the input category \mathcal{C} [57]. For the case, $m_{\mathcal{R}} = m_{\overline{\mathcal{R}}} = 1$, considered here, this expression of the entropy gives $I_{\text{topo}}(T=\infty) = -S_{\mathcal{R} \cup \overline{\mathcal{R}},\text{topo}} = -\ln M$ (see Ref. [57]). Interestingly, this expression is similar to Eq. (72) and in agreement with our expression of the constant (topological) term in Eq. (41) provided $M = M_0$. It turns out that the input categories considered in Ref. [57] are either Abelian or modular. In both cases, it is easy to prove that $M_0 = M$. However, in general, M_0 and M may be different. For instance, if $\mathcal{C} = \text{Rep}(S_3)$, one has $M = 2$ (since the group S_3 has two one-dimensional irreducible representations), but $M_0 = 1$ (since the only pure fluxon in $\mathcal{Z}[\text{Rep}(S_3)]$ is the vacuum [38]).

C. Zero-temperature limit

In the zero- T limit, every plaquette is in the vacuum ($A = \mathbf{1}$) state. Thus, $\langle P_A(L_c) \rangle$ is given by Eq. (50) and one readily gets from Eq. (70):

$$I_{\text{topo}}(T=0) = -2 \ln \mathcal{D}, \quad (74)$$

which is the well-known zero-temperature result for a topological phase with total quantum dimension \mathcal{D} [52, 53, 56].

D. Finite temperature and scaling behavior

Away from the two extreme cases discussed above, the situation is more subtle. As can already be inferred from

Eq. (51), using the same arguments as in the previous section, one always gets

$$\lim_{N_p^{\mathcal{R}}, N_p^{\overline{\mathcal{R}}} \rightarrow \infty} I_{\text{topo}}(T>0) = -\ln M_0, \quad (75)$$

which is also the infinite-temperature limit [see Eq. (72)]. This indicates that topological quantum order is destroyed in the thermodynamic limit for any $T > 0$ as anticipated by Hastings [25]. This phenomenon is similar to the one observed in the toric code [13] (see Refs. [26, 27, 55, 56]).

For a given contour L_c , one observes a crossover between a low- T region where $I_{\text{topo}} \simeq -2 \ln \mathcal{D}$, and a high- T region where $I_{\text{topo}} \simeq -\ln M_0$ (see Fig. 8). When increasing the system size (while keeping L_c fixed), I_{topo} converge towards a unique curve (not shown). The crossover temperature can be estimated from Eq. (51) as follows.

The dominant behavior of $\langle P_X(L_c) \rangle$ in the thermodynamic limit comes from pure fluxons and is given in Eq. (71). The first finite-size correction comes from the nonpure fluxon (call it C) with largest ratio $n_{C,1}/d_C < 1$:

$$\langle P_X(L_c) \rangle - \frac{d_X^2}{\mathcal{D}^2} M_0 \simeq \frac{d_X d_C}{\mathcal{D}} S_{\bar{X},C} e^{-N_p^{\overline{\mathcal{R}}}/N_p^*}, \quad (76)$$

with the characteristic area

$$N_p^* = \max_{A \notin \mathcal{P}} N_A^* = \left[\ln \left(\frac{\mathcal{D} - 1 + e^\beta}{\mathcal{D} \frac{n_{C,1}}{d_C} - 1 + e^\beta} \right) \right]^{-1}, \quad (77)$$

where N_A^* is given in Eq. (67). The quantity N_p^* reaches a constant $1/\ln \frac{d_C}{n_{C,1}}$ in the high- T limit and diverges as

$$N_p^* \simeq \frac{e^\beta}{\mathcal{D}(1 - \frac{n_{C,1}}{d_C})} \quad (78)$$

in the low- T limit. The crossover temperature is reached when $N_p^* \simeq N_p^{\overline{\mathcal{R}}}$ and is roughly given by

$$T_c \simeq \frac{1}{\ln[N_p^{\overline{\mathcal{R}}} \mathcal{D}(1 - n_{C,1}/d_C)]} \simeq \frac{1}{\ln N_p^{\overline{\mathcal{R}}}} \quad (79)$$

when $N_p^{\overline{\mathcal{R}}}$ is large. Such a behavior is analogous to that of the 1D classical Ising model, which has a vanishing critical temperature. That the toric code model is in the same universality class as the 1D classical Ising model is well-known, see e.g. [58]. Here, we suspect that this is also the case of the SN model for any input category.

A close inspection shows a nontrivial interplay between the temperature T and the total system size $N_p = N_p^{\mathcal{R}} + N_p^{\overline{\mathcal{R}}}$, similar to the one found in Refs. [26, 55, 56] for the toric code. More precisely, if one sets $N_p^{\overline{\mathcal{R}}} = \nu N_p$, with a fixed ratio, $0 < \nu < 1$, one can show that, in the large- N_p limit, I_{topo} depends on ν and on the proper scaling variable N_p/N_p^* , where N_p^* is defined in Eq. (77).

Such a scaling law is similar to the one observed in Refs. [26, 55, 56] for the toric code and indicates that

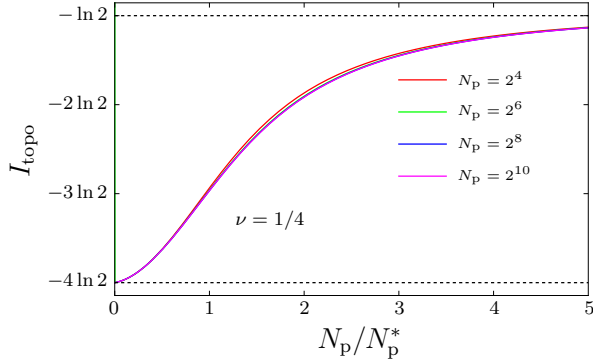


FIG. 9. Topological mutual information of the Ising SN model as a function of the scaling variable N_p/N_p^* at fixed $\nu = 1/4$, where N_p^* is defined in Eq. (77).

topological quantum order can persist at finite temperature provided the system size is small enough. Differences between the Kitaev quantum double and the SN models will be discussed elsewhere.

We display in Fig. 8 the topological mutual information I_{topo} as a function of the inverse temperature for various system sizes at ratio $\nu = 1/4$. One clearly observes that when the system size N_p increases, the topological order characterized by $I_{\text{topo}} = -4 \ln 2$ is destroyed at a temperature which decreases and vanishes in the thermodynamic limit. However, when plotted as a function of the scaling variable N_p^* (see Fig. 9), I_{topo} converges towards a “universal” function which interpolates between $-4 \ln 2$ at $T = 0$ [see Eq. (74)] and $-\ln 2$ at $T = \infty$ [see Eq. (72)].

In summary, the crossover line $N_p^* = N_p^{\overline{\mathcal{R}}}$ separates two domains in the $(T, N_p^{\overline{\mathcal{R}}})$ plane: a low- T and small- $N_p^{\overline{\mathcal{R}}}$ domain with $I_{\text{topo}} \simeq -2 \ln \mathcal{D}$ (indicative of topological order), and a high- T and large- $N_p^{\overline{\mathcal{R}}}$ domain with $I_{\text{topo}} \simeq -\ln M_0$ (absence of topological order).

IX. CONCLUSIONS AND PERSPECTIVES

In the present work, we studied the finite-temperature properties of RSN model which is an extension of the original SN model. Using an exact expression of the degeneracies obtained in a companion paper (see Ref. [38]), we provided a simple and exact expression of the partition function [see Eq. (16)] which is valid for any UFC, any trivalent graph, and any orientable closed surface. This partition function allowed us to analyze the finite-temperature behavior of several quantities. In particular, using simple surgery arguments, we computed the thermal average of the projector onto a given particle sector for three different types of closed loop: handle, throat, and contractible [see Eq. (44) and Fig. 5, Eq. (48) and Fig. 3, and Eq. (49), respectively]. These projectors are directly related to WWL operators [see Eq. (54)] which

provide some information about the confinement of the excitations. Interestingly, these projectors are the key ingredients to compute the topological mutual information according to a conjecture [see Eq. (70)] proposed by Iblisdir *et al.* [55, 56].

Our main finding is that, as seen from different probes (such as the specific heat, confinement, or entanglement), topological order does not survive at $T > 0$ in the thermodynamic limit. This is in line with exact results [25]. However, we find that there is a scaling behavior between the temperature and the system size, generalizing what was found by Iblisdir *et al.* [26, 27, 55, 56]. This is essentially the same scaling as that of the 1D classical Ising model.

Importantly, we have identified different subsets of objects in the Drinfeld center $\mathcal{Z}(\mathcal{C})$ that play a special role: pure fluxons \mathcal{P} that drive the thermodynamic limit and braid trivially with all fluxons, the fluxons \mathcal{F} that characterizes plaquette excitations, and the fusion product of fluxons \mathcal{F}^{\otimes} (see Appendix A for more details). The content of these subsets not only depends on the Drinfeld center, but also on the input category. In other words, two categories with the same Drinfeld center (i.e., Morita equivalent) may have different such subsets.

We have also shown that the Drinfeld center $\mathcal{Z}(\mathcal{C})$ is enough to understand the $T = 0$ or ground-state properties, but that it is not sufficient to analyze properties at finite temperature. For the latter, one needs to know more information that depends on the input category \mathcal{C} . More precisely, one needs to determine the internal multiplicities $n_{A,1}$ from the tube algebra. Perhaps this is not surprising given our prior work in Ref. [38] where we showed that the nontopological degeneracies of the string net models depend on $n_{A,1}$.

For future work we plan on studying models featuring all types of excitations in the Drinfeld center (not only fluxons). This could be done, for instance, in the Kitaev quantum double model [13] or in the extended Levin-Wen model [36], both allowing vertex excitations. Such a study will allow us to analyze the interplay between the various excitations of topologically ordered phases.

ACKNOWLEDGMENTS

We thank N. Bultinck, B. Douçot, S. Iblisdir and L. Lootens, for fruitful discussions. We acknowledge the financial support of the Emergence programs iMAT and TQCNA at Sorbonne Université, Paris.

Appendix A: Fluxons, pure fluxons and fusion product of fluxons

Simple objects A of the Drinfeld center $\mathcal{Z}(\mathcal{C})$ index anyon types, among which we can still distinguish subtypes (A, s) which are, in addition, indexed by an object $s \in \mathcal{C}$ [36]. These subtypes also correspond to “diagonal

sectors” of the tube algebra (see Appendix B). Fluxons (or plaquette excitations) are identified as those subtypes which are indexed by the identity of \mathcal{C} , $(A, 1)$. The multiplicities $n_{A,s}$ count the number of subtypes (A, s) inside an anyon A . Therefore, another way to define fluxons (elements of \mathcal{F}) is

$$A \in \mathcal{F} \Leftrightarrow n_{A,1} > 0. \quad (\text{A1})$$

Among fluxons, we distinguish “pure fluxons” (elements of \mathcal{P}) [36] defined as

$$A \in \mathcal{P} \Leftrightarrow n_{A,1} = d_A. \quad (\text{A2})$$

Since $d_A = \sum_s n_{A,s} d_s$, where d_s are the quantum dimensions of the simple objects in \mathcal{C} and d_A the quantum dimensions of the anyons $A \in \mathcal{Z}(\mathcal{C})$, this means that a pure fluxon contains only the subtype corresponding to the trivial input object $n_{A,s} = d_A \delta_{s,1}$, hence its name.

Below, we prove that this definition (A2) is equivalent to the following:

$$A \in \mathcal{P} \Leftrightarrow S_{A,B} = \frac{d_A d_B}{\mathcal{D}}, \quad \forall B \in \mathcal{F}. \quad (\text{A3})$$

This means that the braiding between a pure fluxon and a fluxon is trivial so that one may unknot the A and B loops in the definition of the S -matrix leading to Eq. (A3) (see, e.g. Fig. 6 in [38]). In other words, a pure fluxon is transparent to all fluxons (but not necessarily to nonfluxons). A corollary (from the hexagon equation [45, 46]) is that Eq. (A3) also holds if A is a pure fluxon and B is any fusion product of fluxons ($B \in \mathcal{F}^\otimes$). Obviously, the three sets \mathcal{P} , \mathcal{F} and \mathcal{F}^\otimes are such that:

$$\{1\} \subseteq \mathcal{P} \subseteq \mathcal{F} \subseteq \mathcal{F}^\otimes \subseteq \mathcal{Z}(\mathcal{C}). \quad (\text{A4})$$

From Eqs. (43) and (71) one obtains the following equality

$$\sum_{A \in \mathcal{Z}(\mathcal{C})} d_A^2 = \sum_{B \in \mathcal{P}} d_B^2 \times \sum_{C \in \mathcal{F}^\otimes} d_C^2, \quad (\text{A5})$$

and the corresponding inequality

$$\mathcal{D}^2 \geq M_0 |\mathcal{F}^\otimes|, \quad (\text{A6})$$

which relates the number of quasiparticles that can be obtained by fusion of fluxons, $|\mathcal{F}^\otimes|$, to the total quantum dimension \mathcal{D} and to M_0 (which, in the case of a commutative input category, is the number of pure fluxons). It shows that when M_0 is small $|\mathcal{F}^\otimes|$ is large and vice-versa.

1. Pure fluxons braid trivially with fluxons

We now prove that (A3) and (A2) are equivalent.

It is easy to prove that the right-hand side (r.h.s.) of Eq. (A3) implies the r.h.s. of Eq. (A2). We start from the fluxon identity (23) [38]

$$n_{A,1} = \sum_{B \in \mathcal{Z}(\mathcal{C})} S_{A,B} n_{B,1} = \sum_{B \in \mathcal{F}} S_{A,B} n_{B,1}, \quad (\text{A7})$$

and note that, on the r.h.s., only fluxons play a role. Therefore, if A is a pure fluxon, we can use Eq. (A3) in the r.h.s. to get

$$n_{A,1} = \sum_{B \in \mathcal{F}} \frac{d_A d_B}{\mathcal{D}} n_{B,1} = d_A \frac{1}{\mathcal{D}} \sum_{B \in \mathcal{F}} d_B n_{B,1}. \quad (\text{A8})$$

Then, we can use Eq. (A7) again for the special case $A = 1$ ($n_{1,1} = 1$), to prove that:

$$\frac{1}{\mathcal{D}} \sum_{B \in \mathcal{F}} d_B n_{B,1} = 1, \quad (\text{A9})$$

and we obtain Eq. (A2). More generally, one has [59]

$$\frac{1}{\mathcal{D}} \sum_{B \in \mathcal{Z}(\mathcal{C})} d_B n_{B,s} = d_s. \quad (\text{A10})$$

for all $s \in \mathcal{C}$.

In order to prove that the r.h.s. of Eq. (A2) implies the r.h.s. of Eq. (A3), we start from the following expression for the S -matrix (see, e.g., Eq. (223) in Ref. [45])

$$S_{A,B} = \frac{1}{\mathcal{D}} \sum_{C \in \mathcal{Z}(\mathcal{C})} N_{A,B}^C \frac{\theta_C}{\theta_A \theta_B} d_C, \quad (\text{A11})$$

which we apply to the case where $A \in \mathcal{P}$ and $B \in \mathcal{F}$. As fluxons, A and B have trivial twists ($\theta_A = \theta_B = 1$). Indeed, the vector \mathbf{n}_1 with components $n_{C,1}$ ($n_{C,1} = 0$, if $C \notin \mathcal{F}$) [38], also obeys $T \cdot \mathbf{n}_1 = \mathbf{n}_1$, where the twist T -matrix is defined by $T_{AB} = \theta_A \delta_{AB}$ (see, e.g., Ref. [38]). Thus, Eq. (A11) gives

$$S_{A,B} = \frac{1}{\mathcal{D}} \sum_{C \in \mathcal{Z}(\mathcal{C})} N_{A,B}^C \theta_C d_C. \quad (\text{A12})$$

Then, we use the fact that the fusion of a pure fluxon A with a fluxon B can only be a fluxon (see below) so that $\theta_C = 1$ and one further gets

$$S_{A,B} = \frac{1}{\mathcal{D}} \sum_{C \in \mathcal{Z}(\mathcal{C})} N_{A,B}^C d_C = \frac{d_A d_B}{\mathcal{D}}, \quad (\text{A13})$$

which completes the proof.

2. Fusion of pure fluxon with fluxon gives fluxon

In order to prove that the fusion product of a pure fluxon and a fluxon can only be a fluxon, we use the fusion of tubes as described in detail in Appendix B. The crux of the argument is the following. We consider the fusion of two anyon subtypes (A, r) and (B, s) that results in some (C, t) , where A, B, C are in $\mathcal{Z}(\mathcal{C})$ and r, s, t are in \mathcal{C} . If A is a pure fluxon then it only contains the trivial input string, i.e. $r = 1$. The fusion of $(A, 1)$ with (B, s) necessarily gives $(A \times B, 1 \times s) = (A \times B, s)$ so

that $C \in A \times B$ and $t = s$. If B is a fluxon ($n_{B,1} > 0$), it means that it contains, at least, $s = 1$. Hence, the particle C also has this sector $t = s = 1$, which means that C is also a fluxon.

As a corollary, we see that if A and B are both pure fluxons (i.e., if $r = 1$ and $s = 1$ are the only nonvanishing sectors), than C must be a pure fluxon as well. In other words, pure fluxons are closed under fusion and therefore form a subcategory. This fusion category is also unitary and symmetric (and not modular). As all fluxons are bosons (i.e. have a trivial twist), we can use the known result that a symmetric fusion category made of bosons is equivalent to a $\text{Rep}(G)$ category, see e.g. [46].

Appendix B: Fusion of tubes

In this Appendix we compute the fusion outcome C of two anyons A and B using the tube algebra. We also show that if A is a pure fluxon and B is a fluxon, then necessarily C is also a fluxon (as anticipated above).

a. Fusion rules from the tube algebra

One way to obtain the fusion rules from the tube algebra is to use the half-braidings to compute the S –matrix and to use the Verlinde formula to obtain the N –matrices. This is the way followed, e.g., in Refs [14, 32, 38]. Here, we follow a different path and obtain the fusion coefficients for the Drinfeld center directly from the tube algebra, without using the half-braidings.

We follow the general strategy described in Sec. V in Ref. [60] (see also Sec. IV in Ref. [61]). For simplicity, we concentrate on commutative and self-dual input categories, but the method can easily be generalized to the non-self-dual and noncommutative case. The first one only requires to put arrows on all strings, where reversing an arrow means going from an object $i \in \mathcal{C}$ to its dual. The second one implies to label sectors of the tube algebra by two indices r, a instead of one r , and to consider particles with $n_{A,1} \geq 1$ (see Appendix A in Ref. [38] for more details). In the following, by convention, we will denote simple objects in \mathcal{C} by lowercase letters and simple objects in $\mathcal{Z}(\mathcal{C})$ by capital letters.

The (central) projector P_A on a particle A can be written as

$$P_A = \sum_r p_A^{rr}. \quad (\text{B1})$$

The simple idempotents p_A^{rr} and nilpotents p_A^{rs} decomposes in the tube basis as

$$p_A^{rs} = \sum_{i,j \in \mathcal{C}} M_{A,irsj}^{-1} Q_{irsj}, \quad (\text{B2})$$

where the coefficients M_A^{-1} depending on $A \in \mathcal{Z}(\mathcal{C})$, $r, s \in \mathcal{C}$ label the sectors in the tube algebra, and where

the Q ’s are the tubes. The reverse version of this formula is

$$Q_{irsj} = \sum_A M_{A,irsj} p_A^{rs}. \quad (\text{B3})$$

The M and M^{-1} together verify

$$\sum_{i,j} M_{A,irsj}^{-1} M_{B,irsj} = \delta_{A,B}. \quad (\text{B4})$$

Following Ref. [32], we represent a one-quasiparticle basis state $|A, a\rangle$, with $A \in \mathcal{Z}(\mathcal{C})$ and $a \in \mathcal{C}$, as in Fig. 10. The dimension of the corresponding Hilbert space is:

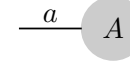


FIG. 10. A single quasiparticle basis state $|A, a\rangle$ corresponding to a simple idempotent $p_A^{aa} = |A, a\rangle \langle A, a|$, with $A \in \mathcal{Z}(\mathcal{C})$ and $a \in \mathcal{C}$.

$$\dim \mathcal{H}_{1\text{QP}} = \sum_{A,a} n_{A,a}. \quad (\text{B5})$$

The action of a tube on this basis state, as represented on Fig. 11, is

$$Q_{irsj}|A, a\rangle = \delta_{r,a} M_{A,irsj}|A, s\rangle. \quad (\text{B6})$$

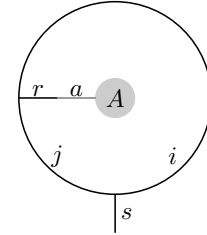


FIG. 11. Action of a tube on a one-quasiparticle state $|A, a\rangle$.

We now introduce a basis for a two-quasiparticle state. We write a state in this basis $|A, a, B, b, c\rangle$ and represent it graphically as in Fig. 12.

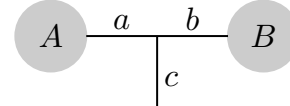
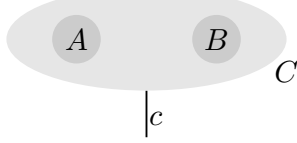


FIG. 12. A two-quasiparticle state $|A, a, B, b, c\rangle$.

In other words, a two-quasiparticle state is entirely fixed if we specify the two quasiparticle types A and B , their tube-algebra sectors a and b , and the channel c in which a and b fuse. An alternative way to describe the two-quasiparticle Hilbert space is to take states $|A, B, C, c\rangle$ as a basis (see Fig. 13). Here, we fix A, B and

FIG. 13. A two-quasiparticle state $|A, B, C, c\rangle$.

their fusion outcome C as well as the tube algebra sector c of C . These states are eigenvectors of the simple idempotents p_C^{cc} :

$$p_{C'}^{c'c'}|A, B, C, c\rangle = \delta_{c,c'}\delta_{C,C'}|A, B, C, c\rangle. \quad (\text{B7})$$

The dimension of the two-quasiparticle Hilbert space is

$$\dim \mathcal{H}_{2\text{QP}} = \sum_{A, B, a, b, c} N_{a,b}^c n_{A,a} n_{B,b}, \quad (\text{B8})$$

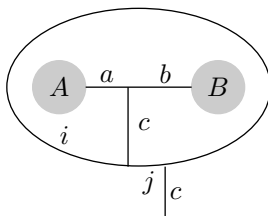
$$= \sum_{A, B, C, c} N_{A,B}^C n_{C,c}. \quad (\text{B9})$$

The equality between these two lines follows from the commutation between fusion and restriction in anyon condensation [59]. Since

$$\sum_{A, B, a, b} n_{A,a} n_{B,b} \sum_c N_{a,b}^c \geq \sum_{A, B, a, b} n_{A,a} n_{B,b}, \quad (\text{B10})$$

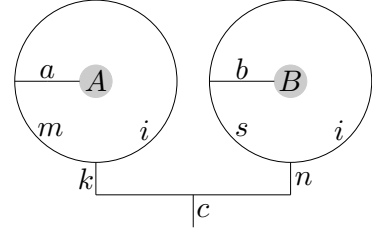
the dimension of the two-quasiparticle Hilbert space (B8) is larger than the square of the dimension of the one-quasiparticle Hilbert space (B5), which is a signature of entanglement.

The action of a tube Q_{iccj} on a state $|A, a, B, b, c\rangle$ can graphically be represented as in Fig. 14. Applying a se-

FIG. 14. Tube Q_{iccj} acting on $|A, a, B, b, c\rangle$.

ries of F -moves, this diagram can be modified into the diagram of Fig. 15. In this figure, the diagram of the big tube around A and B has been reduced to two smaller tubes, one tube Q_{iakm} around A and Q_{ibns} around B . Using finally Eq. (B6) we see that we can write

$$Q_{iccj}|A, a, B, b, c\rangle = \sum_{i,j,s,r, k,m,n} F_{aar}^{ii0} F_{bbs}^{ii0} F_{air}^{sib} F_{ijk}^{src} F_{cin}^{skj} F_{ikm}^{iar} \times \sqrt{\frac{d_i d_a}{d_r}} M_{A, iakm} M_{B, ibns} |A, k, B, n, c\rangle. \quad (\text{B11})$$

FIG. 15. Same as Fig. 14 after a series of F -moves. Now, there are two tubes Q_{iakm} and Q_{ibns} acting on single quasiparticle states $|A, a\rangle$ and $|B, b\rangle$.

The action of a simple idempotent p_C^{cc} on such a state is therefore

$$\begin{aligned} p_C^{cc} |A, a, B, b, c\rangle &= \sum_{i,j,s,r, k,m,n} M_{C, iccj}^{-1} F_{aar}^{ii0} F_{bbs}^{ii0} F_{air}^{sib} F_{ijk}^{src} \\ &\quad \times F_{cin}^{skj} F_{ikm}^{iar} \sqrt{\frac{d_i d_a}{d_r}} M_{A, iakm} M_{B, ibns} |A, k, B, n, c\rangle \\ &= \sum_{k,n} \mathcal{M}_{kn,ab} |A, k, B, n, c\rangle, \end{aligned} \quad (\text{B12})$$

where, in the last line, we have introduced the matrix-like notation:

$$\begin{aligned} \mathcal{M}_{kn,ab}(A, B, C, c) &= \sum_{i,j,s, r,m} F_{aar}^{ii0} F_{bbs}^{ii0} F_{air}^{sib} F_{ijk}^{src} F_{cin}^{skj} F_{ikm}^{iar} \\ &\quad \times \sqrt{\frac{d_i d_a}{d_r}} M_{C, iccj}^{-1} M_{A, iakm} M_{B, ibns}. \end{aligned}$$

An important property of Eq. (B12) is that A , B and c are fixed and that only a and b are mixed into k and n .

The identity operator is obtained by summing Eq. (B12) over all c and C :

$$\sum_{C,c} p_C^{cc} |A, a, B, b, c\rangle = |A, a, B, b, c\rangle. \quad (\text{B13})$$

We can construct the eigenvectors of p_C^{cc} by solving the equation

$$\sum_{a,b} \mathcal{M}_{kn,ab} y_{ab} = y_{kn}, \quad (\text{B14})$$

for all y_{kn} , where

$$|A, B, C, c\rangle = \sum_{a,b} y_{ab} |A, a, B, b, c\rangle. \quad (\text{B15})$$

Since for every quasiparticle C there is a unique linear combination of the states $|A, a, B, b, c\rangle$, the trace of p_C^{cc} over a and b is always 1 (if C is a fusion outcome of A and B , i.e., the state $|A, B, C, c\rangle$ exists), and zero otherwise:

$$\begin{aligned} \sum_{a,b} \langle A, a, B, b, c | p_C^{cc} |A, a, B, b, c\rangle &= \sum_{a,b} \mathcal{M}_{ab,ab} \\ &= \begin{cases} 1, & \text{if } C \in A \times B \\ 0, & \text{otherwise.} \end{cases} \end{aligned} \quad (\text{B16})$$

This is the key equation that allows one to obtain the fusion rules, i.e., $N_{A,B}^C$ of the Drinfeld center from the tube algebra.

We also have

$$\text{Tr}_{a,b}(P_C) = \sum_{a,b,c} \mathcal{M}_{ab,ab} = n_C. \quad (\text{B17})$$

The dimension of the two-quasiparticle Hilbert space can be recovered by computing

$$\dim \mathcal{H}_{2\text{QP}} = \sum_{A,B,C,a,b,c} \mathcal{M}_{ab,ab}. \quad (\text{B18})$$

b. Fusion of a pure fluxon with a fluxon

We now aim at showing that the product of a pure fluxon with another fluxon necessarily gives a fluxon. In the following, we will take A to be a pure fluxon. All its tubes are contained only in the sector 11, so that Eq. (B16) simplifies to (using identities on the F -symbols):

$$\delta_{c,b} \sum_{i,j} M_{C,ibbj}^{-1} \frac{1}{d_i} M_{A,i11i} M_{B,ibbj} = \begin{cases} 1, & \text{if } C \in A \times B \\ 0, & \text{otherwise.} \end{cases} \quad (\text{B19})$$

for any sector b of B . In particular, for $b = 1$, we have

$$\sum_i M_{C,i11i}^{-1} \frac{1}{d_i} M_{A,i11i} M_{B,i11i} = 1 \quad (\text{B20})$$

when $C \in A \times B$. If B is a fluxon, there is necessarily some i for which $M_{B,i11i}$ is nonvanishing. In order to satisfy equation Eq. (B20), we then see that C must have some nonvanishing $M_{C,i11i}^{-1}$, which means it has weight on the 11 sector and is also a fluxon.

We can go further when the pure fluxon A is the vacuum. In this case, we have a simple expression for $M_{1,i11i} = d_i$, so that Eq. (B19) becomes

$$\sum_{i,j} M_{C,ibbj}^{-1} M_{B,ibbj} = 1. \quad (\text{B21})$$

Using Eq. (B4), we see that Eq. (B21) is true only when $C = B$, as it is expected for the fusion with the vacuum.

c. Example: Fibonacci

As an example, let us consider the case where \mathcal{C} is the Fibonacci category. It is a non-Abelian UMTC which contains two objects, 1 and τ . As a UMTC, its Drinfeld center is built as the direct product $\mathcal{C} \times \bar{\mathcal{C}}$ where $\bar{\mathcal{C}}$ is the mirror image of \mathcal{C} (opposite chirality) (see, e.g., Ref. [62] for more details).

There are five one-quasiparticle states $|A, a\rangle$: $|(1, 1), 1\rangle$, $|(1, \tau), \tau\rangle$, $|(\tau, 1), \tau\rangle$, $|(\tau, \tau), 1\rangle$, $|(\tau, \tau), \tau\rangle$, while there are

34 two-quasiparticle states. Let's look in particular at the case where $A = (\tau, \tau)$, $B = (\tau, \tau)$ and $c = 1$. In this subspace, we have two states written in the $|A, a, B, b, c\rangle$ basis as:

$$\begin{aligned} |a_1\rangle &= |(\tau, \tau), 1, (\tau, \tau), 1, 1\rangle, \\ |a_2\rangle &= |(\tau, \tau), \tau, (\tau, \tau), \tau, 1\rangle, \end{aligned} \quad (\text{B22})$$

while in the basis $|A, B, C, c\rangle$ the two states are

$$\begin{aligned} |b_1\rangle &= |(\tau, \tau), (\tau, \tau), (1, 1), 1\rangle, \\ |b_2\rangle &= |(\tau, \tau), (\tau, \tau), (\tau, \tau), 1\rangle. \end{aligned} \quad (\text{B23})$$

The relation between the two bases are:

$$|b_1\rangle = \frac{1}{\sqrt{2}}(|a_1\rangle - |a_2\rangle), \quad (\text{B24})$$

$$|b_2\rangle = \sqrt{\frac{2}{5 + \sqrt{5}}} |a_1\rangle + \sqrt{\frac{5 + \sqrt{5}}{10}} |a_2\rangle. \quad (\text{B25})$$

For other choices of A , B and c there might exist only one state in which case the two bases are equivalent. For example, when $A = (1, 1)$, $B = (1, 1)$ and $c = 1$, one has

$$|(1, 1), 1, (1, 1), 1, 1\rangle = |(1, 1), (1, 1), (1, 1), 1\rangle. \quad (\text{B26})$$

Appendix C: Surgery approach to degeneracies

In this appendix, our objective is to calculate the degeneracy of a state of a (2+1)D TQFT on a g -handled torus Σ_g , with the following possible complications: (a) We may have quasiparticles at fixed positions on the torus; (b) We may have WWL operators running around one of the (space-like) handles. We will do this calculation with some nice TQFT and topological techniques. Our calculation will give the topological degeneracies of a pure TQFT and will not account for the nontopological degeneracies of the SN model. Hence our result will only be precise for the case of the Drinfeld center of a commutative UFC where there are no nontopological degeneracies. For the quantum double of noncommutative UFCs, the nontopological degeneracies would have to be added to the expressions by hand. In this way, we will recover many results of the main text in an alternative way and without explicit reference to a specific lattice model such as the SN or RSN.

We will consider a (closed) three-dimensional space-time manifold of the form $\mathcal{M} = \Sigma_g \times S^1$, where Σ_g is the g -handled torus which will be our space-like manifold and S^1 is a time-like circle. We are going to describe this manifold using “surgery.” It turns out (see Refs. [63, 64]) that any orientable 3-manifold can be obtained by starting with the 3-sphere S^3 and doing *surgery* on some link (in the sense of knot theory) embedded in S^3 (this fact is known as the “Lickorish-Wallace Theorem”[65–67]). By “surgery” we mean the following procedure (see the discussion in Refs. [46, 63] for example): (a) Thicken

each strand of the link into a solid torus $S^1 \times D^2$ with D^2 the disc (b) For each strand remove this solid torus from the manifold and (c) for each $S^1 \times D^2$ removed, insert instead a new solid torus $D^2 \times S^1$, i.e., switch the contractible and noncontractible directions.

It is a known fact from topology that the manifold $\Sigma_g \times S^1$ is given by surgery on the knot shown in Fig. 16 (only the black pieces) where all the strands are 0-framed, meaning they have no self-twists. This fact is given explicitly (and the derivation explained) in Fig. 6.4 of Ref. [63] (to be precise, in that figure they are using the same diagram to describe the 4-manifold that is bounded by our 3-manifold of interest, however the diagram is the same to just describe the 3-manifold, see also Ref. [64]). To give some intuition behind this topological statement, surgery on a single loop turns S^3 into the manifold $S^2 \times S^1$, i.e., it generates one noncontractible loop (the S^1) (see Ref. [46] chapter 24 for example). Similarly, if we ignore the long string in Fig. 16 we have $2g$ unlinked loops, and surgery on all of these unlinked loops generates the so-called “connected-sum” of $2g$ factors of $S^2 \times S^1$. (A “connected-sum” of two three-manifolds \mathcal{M}_1 and \mathcal{M}_2 is given by removing a ball from each manifold to form $\mathcal{M}_1 \setminus B^3$ and $\mathcal{M}_2 \setminus B^3$ with the notation \setminus meaning “remove”. Then we sew $\mathcal{M}_1 \setminus B^3$ and $\mathcal{M}_2 \setminus B^3$ together on the spherical surfaces that have been exposed to form the connected-sum which is notated $\mathcal{M}_1 \# \mathcal{M}_2$.) The resulting manifold has $2g$ independent noncontractible loops. The small red loop, after the surgery, goes around one of these noncontractible loops. The final surgery on the long loop adds one more noncontractible direction (this is the time-like S^1) and after surgery the blue loop goes around this noncontractible direction. Note that this last loop is now not independent of the other noncontractible loops — and indeed, ties the other directions together in pairs — and generates a nontrivial fundamental group after the surgery. For the case of $g = 1$, the knot in Fig. 16 is the borromean rings and surgery gives the three-torus with Σ_g just the usual single-handled torus[63, 64].

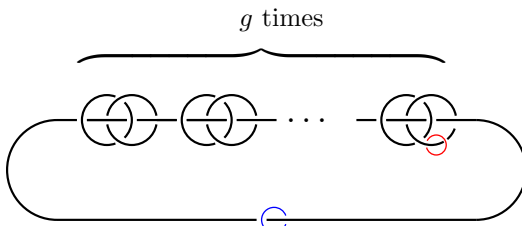


FIG. 16. Without the small blue and red loops, this link (0-framed, meaning no line has any self twists) is the surgery presentation of the 3-manifold $\Sigma_g \times S^1$ where Σ_g is a g -handled torus. The blue loop is a loop in the S^1 or time-like direction after surgery. The red loop is a noncontractible space-like loop on the g -handled torus after surgery.

Now, as discussed in Refs. [46, 68] the degeneracy of states on Σ_g is given by the partition function of the

TQFT on the 3-manifold $\Sigma_g \times S^1$

$$\begin{aligned} \text{Number of States } (\Sigma_g) &= \text{Tr} \left[\sum_{\text{states}} |\text{state}\rangle \langle \text{state}| \right], \\ &= \mathcal{Z}(\Sigma_g \times S^1). \end{aligned} \quad (\text{C1})$$

Here we have used the notation \mathcal{Z} for a TQFT partition function, as for example used by Witten [68]. We use mathscript font here so as not to confuse this quantity with the finite temperature partition functions Z in the main text or the Drinfeld center \mathcal{Z} .

The expression, Eq. (C1), remains true even if there are particles at fixed positions on Σ_g (we just absorb these particles into the definition of Σ_g and it is exactly the same equation). For a WWL operator labeled with particle type w going around a (space-like) noncontractible loop L , we need to add such a loop into the 3D manifold when we calculate the partition function

$$\begin{aligned} \langle W_w(L) \rangle &= \text{Tr} \left[W_w(L) \sum_{\text{states}} |\text{state}\rangle \langle \text{state}| \right], \\ &= \mathcal{Z}(\Sigma_g \times S^1 \text{ with loop } w \text{ around handle } L). \end{aligned} \quad (\text{C2})$$

To calculate these partition functions we use the Reshetikhin-Turaev [46, 69] approach — that is, we represent the manifold $\Sigma_g \times S^1$ with the above-mentioned surgery presentation, we label each surgery loop with the Kirby strand Ω [see Eq. (58)] and then simply calculate the diagram that results using the usual TQFT (modular tensor category) evaluation rules. If there are also additional particle lines in the picture (say the red or blue lines going around handles) these can be evaluated using the TQFT evaluation rules as well. The general result is

$$\mathcal{Z}(\mathcal{M}, \text{labeled link}) = \frac{e^{i\phi}}{\mathcal{D}} (\text{Diagram Evaluation}), \quad (\text{C3})$$

where $\mathcal{D} = \sqrt{\sum_a d_a^2}$ is the total quantum dimension of the TQFT and the phase ϕ for our purposes is going to be zero (in general the phase depends on the so-called “signature” of the surgery Ω link. However that is zero here since none of the strands are linked with each other and none of the strands have self-twists).

In evaluating the diagram we will make extensive use of the so-called “killing” property of the Ω loop: The value of an (untwisted) Ω loop is \mathcal{D} if there is no net particle going through the loop (i.e., the total quantum number going through is zero) and the value of the diagram is zero otherwise. Using the definition of Ω , the completeness relation of Fig. 17, and the killing property we have the graphical equality shown in Fig. 18

Thus using the relation in Fig. 18 a total of g times, the picture in Fig. 16 (ignoring red and blue loops) is reduced to a very simple diagram with a single long Ω loop linked by $2g$ loops labeled $a_1, \bar{a}_1, a_2, \bar{a}_2, \dots, a_g, \bar{a}_g$ with a sum over all the a ’s. We can then merge the loops with each other using the identity shown in Fig. 19.

$$b \Big| \Big| c = \sum_{a,\mu} \sqrt{\frac{d_a}{d_b d_c}} \quad \text{Diagram: } \begin{array}{c} b \\ \mu \\ \mu \\ a \\ b \\ c \end{array}$$

FIG. 17. Completeness relation.

$$\begin{aligned} & - \text{Diagram: } \text{two loops} \\ & = \sum_a \frac{d_a}{\mathcal{D}} - \text{Diagram: } \text{one loop} \\ & = \sum_{a,x} \frac{\sqrt{d_x}}{\mathcal{D}} - \text{Diagram: } \text{two loops} \\ & = \sum_a - \text{Diagram: } \text{two loops} \end{aligned}$$

FIG. 18. The black lines are Ω strands. Going from the first line to the second inserts the definition of Ω for one loop. Going to the third line uses the completeness relation shown in Fig. 17 (vertex indices are not written for simplicity). Going to the final line uses the killing property.

Once all of the a loops are fused together, we use Eq. (C3) to obtain the ground-state degeneracy of a g -handled torus:

$$\begin{aligned} \mathcal{Z}(\Sigma_g \times S^1) &= \frac{1}{\mathcal{D}} \sum_{a_1, \dots, a_g, b} N_{a_1 \bar{a}_1 a_2 \bar{a}_2 \dots a_g \bar{a}_g}^b \text{Diagram: } \text{one loop} \\ &= \sum_{a_1, \dots, a_g} N_{a_1 \bar{a}_1 a_2 \bar{a}_2 \dots a_g \bar{a}_g}^1. \end{aligned} \quad (\text{C4})$$

Note that the black Ω loop in Eq. (C4) is the long Ω loop from Fig. 16. Going to the last line in Eq. (C4) we have used the killing property again. Note that this results agrees with Eq. (7) in the absence of plaquette fluxes.

We now consider how this calculation changes if we add quasiparticles at fixed positions. Such quasiparticles remain in the same position at all time and thus wrap around the time-like S^1 direction of $\Sigma_g \times S^1$. These correspond to the blue ring in Fig. 16. When we calculate $\mathcal{Z}(\mathcal{M}, \text{labeled link})$ the diagram to be evaluated now includes one additional labeled ring around the long Ω loop for every quasiparticle present. These rings may be fused together using Fig. 19 and then also fused with the a, \bar{a} rings as well.

Thus if we have quasiparticles labeled A_1, \dots, A_M on our torus, the degeneracy of states is now

$$\begin{aligned} \mathcal{Z}(\Sigma_g \times S^1; A_1, \dots, A_M) &= \\ & \sum_{a_1, \dots, a_g} N_{a_1 \bar{a}_1 a_2 \bar{a}_2 \dots a_g \bar{a}_g}^1 N_{A_1, A_2, \dots, A_M}^1, \end{aligned} \quad (\text{C5})$$

which agrees with Eq. (7).

$$- \text{Diagram: } \text{two loops} = \sum_c N_{ab}^c - \text{Diagram: } \text{one loop}$$

FIG. 19. Fusion of Loops. See Ref. [46], Figs. 17.1 and 17.3.

Now we consider a WWL operator around a space-like handle, say labeled with w as we consider in Eq. (C2). This corresponds to a labeled loop like the red loop in Fig. 16. Here, one of our a loops that we obtain from Fig. 19 will end up with a red w -loop around it. However, we can then use the unwrapping move shown in Fig. 7 to remove the w loop and accumulate a factor of $S_{w,a}/S_{1,a}$. Thus we obtain

$$\begin{aligned} \mathcal{Z}(\Sigma_g \times S^1; A_1, \dots, A_M; \text{loop } w \text{ around handle 1}) &= \\ \sum_{a_1, \dots, a_g} \frac{S_{w,a_1}}{S_{1,a_1}} N_{a_1 \bar{a}_1 a_2 \bar{a}_2 \dots a_g \bar{a}_g}^1 N_{A_1, A_2, \dots, A_M}^1. \end{aligned} \quad (\text{C6})$$

To compare to the main text we convert the WWL operator to obtain a projector P_X using Eq. (55). This then tells us that the dimension of the space such that only flux X goes around the handle 1 is given by

$$\langle P_X(L_1) \rangle = \sum_{a_2, \dots, a_g} N_{X \bar{X} a_2 \bar{a}_2 \dots a_g \bar{a}_g}^1 N_{A_1, A_2, \dots, A_M}^1, \quad (\text{C7})$$

which also matches the main text Eqs. (7) and (14).

Note that with this approach we can also calculate the expectation of multiple Wilson loops going around different handles. For example,

$$\begin{aligned} \mathcal{Z}(\Sigma_g \times S^1; A_1, \dots, A_M; \text{loop } w_1, w_2 \text{ around handles 1,2}) &= \\ \sum_{a_1, \dots, a_g} \frac{S_{w_1 a_1}}{S_{1,a_1}} \frac{S_{w_2 a_2}}{S_{1,a_2}} N_{a_1 \bar{a}_1 a_2 \bar{a}_2 \dots a_g \bar{a}_g}^1 N_{A_1, A_2, \dots, A_M}^1. \end{aligned} \quad (\text{C8})$$

It is interesting to consider a WWL that follows a throat as in Fig. 2. Let us first imagine that on one side of the throat is a surface of genus 1 and the other side is genus $g-1$.

Let p be a path that follows one nontrivial handle in Fig. 2 and let q be the path following the conjugate handle direction. The path around the cut disk where we put w can be represented as $pqp^{-1}q^{-1}$. In our surgery diagram we would have a WWL as shown in the upper half of Fig. 20. Using the same techniques as in Fig. 18 and Fig. 19 we can evaluate the diagram to obtain the expression in the lower half. The w loop can be removed using the unlinking move to accumulate a factor of $S_{wb}/S_{1,b}$ and we end up with the final result of

$$\begin{aligned} \mathcal{Z}(\Sigma_g \times S^1; A_1, \dots, A_M; \text{loop } w \text{ around } pqp^{-1}q^{-1}) &= \\ \sum_{b, a_1, \dots, a_g} \frac{S_{wb}}{S_{1,b}} N_{a_1 \bar{a}_1}^b N_{b a_2 \bar{a}_2 \dots a_g \bar{a}_g}^1 N_{A_1, A_2, \dots, A_M}^1. \end{aligned} \quad (\text{C9})$$

If we instead have our WWL follow a throat that separates genus g_R from genus $g_{\bar{R}}$ on a $g = g_R + g_{\bar{R}}$ genus

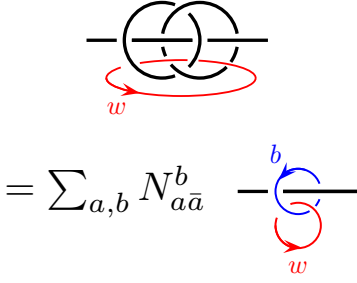


FIG. 20. A WWL around a throat that separates a single handle from the remainder of the handles.

surface, then WWL path can be represented as

$$p_1 q_1 p_1^{-1} q_1^{-1} p_2 q_2 p_2^{-1} q_2^{-1} \cdots p_{g_{\mathcal{R}}} q_{g_{\mathcal{R}}} p_{g_{\mathcal{R}}}^{-1} q_{g_{\mathcal{R}}}^{-1}, \quad (\text{C10})$$

where p_j and q_j are the two conjugate paths around the j^{th} handle. The link analogous to the top of Fig. 20 would have a single red strand threading through $g_{\mathcal{R}}$ pairs of Ω loops before closing. We use the same procedure to evaluate the handle and obtain a figure similar to the lower of Fig. 20 except now the w strand is linked to $g_{\mathcal{R}}$ different b strands which we call $b_1, \dots, b_{g_{\mathcal{R}}}$. The b strands can be fused together to one single loop we call b , then the unlinking move can be invoked. The result of this calculation is

$$\begin{aligned} \mathcal{Z}(\Sigma_g \times S^1; A_1, \dots, A_M; \\ \text{loop } w \text{ around throat separating } g_{\mathcal{R}} \text{ from } g_{\mathcal{R}}) = \\ \sum_{b, a_1, \dots, a_g} \frac{S_{wb}}{S_{1a}} N_{a_1 \bar{a}_1 a_2 \bar{a}_2 \dots a_g \bar{a}_{g_{\mathcal{R}}}}^b \quad (\text{C11}) \\ N_{b a_{g_{\mathcal{R}}+1} \bar{a}_{g_{\mathcal{R}}+1} \dots a_g \bar{a}_g A_1, A_2, \dots, A_M}^1, \end{aligned}$$

Converting this result from a WWL to a projector P_X using Eq. (55) we obtain

$$N_{a_1 \bar{a}_1 a_2 \bar{a}_2 \dots a_g \bar{a}_{g_{\mathcal{R}}}}^X N_{X a_{g_{\mathcal{R}}+1} \bar{a}_{g_{\mathcal{R}}+1} \dots a_g \bar{a}_g A_1, A_2, \dots, A_M}^1, \quad (\text{C12})$$

which matches Eqs. (7) and (12) except that all of the plaquette fluxes have ended up on the $g_{\mathcal{R}}$ side. The reason for this is that we arranged for our WWL link to surround the handles (by linking the red line through the relevant Ω strands), but we did not arrange for them to surround the plaquette fluxes. To move plaquette fluxes to the other side we simply need to link the red WWL through the plaquette flux loops (blue in Fig. 16) as well.

A more interesting case to consider is where we have two Wilson loops going around “conjugate” handles, i.e.,

where projected to the two dimensional surface, the two loops would have to intersect. First, we realize that the temporal order of the two loops cannot matter, since the time-like direction is periodic. We then want to consider Wilson loops around *both* rings at the top of Fig. 18 to indicate that they go around the two conjugate handles created by these two Ω rings after surgery. Let us consider putting a w_1 loop around the left loop at the top of

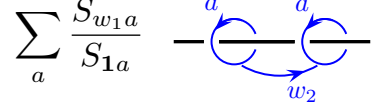


FIG. 21. With Wilson loops w_1 and w_2 around two conjugate handles, instead of Fig. 18 one obtains this.

Fig. 18 and a w_2 loop around the right ring. We follow the same procedure to the second line of Fig. 18 and we can again remove the w_1 ring around the a loop with an unlinking factor of S_{w1a}/S_{1a} . Going to the third line of Fig. 18 the w_2 loop links the small Ω loop. Fortunately, we can use Fig. 17 to fuse w_2 with x inside the small Ω loop and then use the killing property of Ω to obtain Fig. 21 instead of the final diagram of Fig. 18. Further evaluation is fairly straightforward : fuse all other a 's into a single quantum number b and then one has a single (long) Ω loop with three loops wrapped around it: b as well as the a and \bar{a} from Fig. 21. These three can be fused together using Fig. 17 and one can use the killing property of the last Ω . The diagram that remains is a single F symbol.

A simple case to consider is the case of a 1-handle torus with WWL w_1 and w_2 around the two conjugate noncontractible loops. The simplest way to get this is to realize that $\Sigma_g \times S^2$ is a 3-torus, and we can put WWL w_1 and w_2 around any two of the noncontractible loops — so let us put one around a spatial loop and one around a time-like loop. Thus we can invoke the result of Eq. (C6) to give us:

$$\sum_a \frac{S_{w1a}}{S_{1a}} N_{a\bar{a}w_2}. \quad (\text{C13})$$

This does not look very symmetric between the two loops. However, using the Verlinde form of N we obtain:

$$\sum_{a,b} \frac{S_{w1a} S_{w2b} S_{ab} S_{\bar{a}\bar{b}}}{S_{1a} S_{1b}}. \quad (\text{C14})$$

[1] X.-G. Wen, Zoo of quantum-topological phases of matter, *Rev. Mod. Phys.* **89**, 041004 (2017).

[2] D. C. Tsui, H. L. Stormer, and A. C. Gossard, Two-Dimensional Magnetotransport in the Extreme Quantum Limit, *Phys. Rev. Lett.* **48**, 1559 (1982).

[3] J. M. Leinaas and J. Myrheim, On the theory of identical particles, *Nuovo Cim. B* **37**, 1 (1977).

[4] G. A. Goldin, R. Menikoff, and D. H. Sharp, Particle statistics from induced representations of a local current group, *J. Math. Phys.* **21**, 650 (1980).

[5] G. A. Goldin, R. Menikoff, and D. H. Sharp, Representations of a local current algebra in non-simply connected space and the Aharonov-Bohm effect, *J. Math. Phys.* **22**, 1664 (1981).

[6] F. Wilczek, Magnetic flux, angular momentum, and statistics, *Phys. Rev. Lett.* **48**, 1144 (1982).

[7] F. Wilczek, Quantum Mechanics of Fractional-Spin Particles, *Phys. Rev. Lett.* **49**, 957 (1982).

[8] H. Bartolomei, M. Kumar, R. Bisognin, A. Marguerite, J.-M. Berroir, E. Bocquillon, B. Plaçais, A. Cavanna, Q. Dong, U. Gennser, Y. Jin, and G. Fèvre, Fractional statistics in anyon collisions, *Science* **368**, 173 (2020).

[9] J. Nakamura, S. Liang, G. C. Gardner, and M. J. Manfra, Direct observation of anyonic braiding statistics, *Nat. Phys.* **16**, 931 (2020).

[10] T. Werkmeister, J. R. Ehrets, M. E. Wesson, D. H. Najafovabadi, K. Watanabe, T. Taniguchi, B. I. Halperin, A. Yacoby, and P. Kim, Anyon braiding and telegraph noise in a graphene interferometer, [arXiv:2403.18983](https://arxiv.org/abs/2403.18983).

[11] N. L. Samuelson, L. A. Cohen, W. Wang, S. Blanch, T. Taniguchi, K. Watanabe, M. P. Zaletel, and A. F. Young, Anyonic statistics and slow quasiparticle dynamics in a graphene fractional quantum Hall interferometer, [arXiv:2403.19628](https://arxiv.org/abs/2403.19628).

[12] C. Nayak, S. H. Simon, A. Stern, M. Freedman, and S. D. Sarma, Non-Abelian anyons and topological quantum computation, *Rev. Mod. Phys.* **80**, 1083 (2008).

[13] A. Kitaev, Fault-tolerant quantum computation by anyons, *Ann. Phys. (NY)* **303**, 2 (2003).

[14] M. A. Levin and X.-G. Wen, String-net condensation: A physical mechanism for topological phases, *Phys. Rev. B* **71**, 045110 (2005).

[15] C. Song, D. Xu, P. Zhang, J. Wang, Q. Guo, W. Liu, K. Xu, H. Deng, K. Huang, D. Zheng, S.-B. Zheng, H. Wang, X. Zhu, C.-Y. Lu, and J.-W. Pan, Demonstration of Topological Robustness of Anyonic Braiding Statistics with a Superconducting Quantum Circuit, *Phys. Rev. Lett.* **121**, 030502 (2018).

[16] C. K. Andersen, A. Remm, S. Lazar, S. Krinner, N. Lacroix, G. J. Norris, M. Gabureac, C. Eichler, and A. Wallraff, Repeated quantum error detection in a surface code, *Nat. Phys.* **16**, 875 (2020).

[17] Google Quantum AI, Exponential suppression of bit or phase errors with cyclic error correction, *Nature (London)* **595**, 383 (2021).

[18] S. Xu, Z.-Z. Sun, K. Wang, L. Xiang, Z. Bao, Z. Zhu, F. Shen, Z. Song, P. Zhang, W. Ren, X. Zhang, H. Dong, J. Deng, J. Chen, Y. Wu, Z. Tan, Y. Gao, F. Jin, X. Zhu, C. Zhang, N. Wang, Y. Zou, J. Zhong, A. Zhang, W. Li, W. Jiang, L.-W. Yu, Y. Yao, Z. Wang, H. Li, Q. Guo, C. Song, H. Wang, and D.-L. Deng, Digital simulation of projective non-abelian anyons with 68 superconducting qubits, *Chinese Physics Letters* **40**, 060301 (2023).

[19] K. J. Satzinger *et al.*, Realizing topologically ordered states on a quantum processor, *Science* **374**, 1237 (2021).

[20] G. Semeghini, H. Levine, A. Keesling, S. Ebadi, T. T. Wang, D. Bluvstein, R. Verresen, H. Pichler, M. Kalinowski, R. Samajdar, A. Omran, S. Sachdev, A. Vishwanath, M. Greiner, V. Vuletić, and M. D. Lukin, Probing topological spin liquids on a programmable quantum simulator, *Science* **374**, 1242 (2021).

[21] Z. K. Minev, K. Najafi, S. Majumder, J. Wang, A. Stern, E.-A. Kim, C.-M. Jian, and G. Zhu, Realizing string-net condensation: Fibonacci anyon braiding for universal gates and sampling chromatic polynomials, [arXiv:2406.12820](https://arxiv.org/abs/2406.12820).

[22] A. Kapustin and L. Fidkowski, Local commuting projector hamiltonians and the quantum hall effect, *Commun. Math. Phys.* **373**, 763 (2019).

[23] A. Kapustin and L. Fidkowski, Vanishing hall conductance for commuting hamiltonians, *Phys. Rev. B* **105**, L081103 (2022).

[24] S. Bravyi, M. B. Hastings, and S. Michalakis, Topological quantum order: Stability under local perturbations, *J. Math. Phys.* **51**, 093512 (2010).

[25] M. Hastings, Topological Order at Nonzero Temperature, *Phys. Rev. Lett.* **107**, 210501 (2011).

[26] C. Castelnovo and C. Chamon, Entanglement and topological entropy of the toric code at finite temperature, *Phys. Rev. B* **76**, 184442 (2007).

[27] Z. Nussinov and G. Ortiz, Autocorrelations and thermal fragility of anyonic loops in topologically quantum ordered systems, *Phys. Rev. B* **77**, 064302 (2008).

[28] E. Dennis, A. Kitaev, A. Landahl, and J. Preskill, Topological quantum memory, *J. Math. Phys.* **43**, 4452 (2002).

[29] R. Alicki, M. Fannes, and M. Horodecki, On thermalization in Kitaev's 2D model, *J. Phys. A* **42**, 065303 (2009).

[30] O. Landon-Cardinal and D. Poulin, Local Topological Order Inhibits Thermal Stability in 2D, *Phys. Rev. Lett.* **110**, 090502 (2013).

[31] B. J. Brown, D. Loss, J. K. Pachos, C. N. Self, and J. R. Wootton, Quantum memories at finite temperature, *Rev. Mod. Phys.* **88**, 045005 (2016).

[32] T. Lan and X.-G. Wen, Topological quasiparticles and the holographic bulk-edge relation in (2+1)-dimensional string-net models, *Phys. Rev. B* **90**, 115119 (2014).

[33] C.-H. Lin and M. Levin, Generalizations and limitations of string-net models, *Phys. Rev. B* **89**, 195130 (2014).

[34] A. Hahn and R. Wolf, Generalized string-net model for unitary fusion categories without tetrahedral symmetry, *Phys. Rev. B* **102**, 115154 (2020).

[35] C.-H. Lin, M. Levin, and F. J. Burnell, Generalized string-net models: A thorough exposition, *Phys. Rev. B* **103**, 195155 (2021).

[36] Y. Hu, N. Geer, and Y.-S. Wu, Full dyon excitation spectrum in extended Levin-Wen models, *Phys. Rev. B* **97**, 195154 (2018).

[37] A. Kómár and O. Landon-Cardinal, Anyons are not energy eigenspaces of quantum double Hamiltonians, *Phys. Rev. B* **96**, 195150 (2017).

[38] A. Ritz-Zwilling, J.-N. Fuchs, S. H. Simon, and J. Vidal, Topological and nontopological degeneracies in generalized string-net models, *Phys. Rev. B* **109**, 045130 (2024).

[39] J. Vidal, Partition function of the Levin-Wen model, *Phys. Rev. B* **105**, L041110 (2022).

[40] A. P. O. Chan, J. C. Y. Teo, and S. Ryu, Topological phases on non-orientable surfaces: twisting by parity symmetry, *New J. Phys.* **18**, 035005 (2016).

[41] M. Barkeshli, P. Bonderson, M. Cheng, C.-M. Jian, and K. Walker, Reflection and Time Reversal Symmetry Enriched Topological Phases of Matter: Path Integrals, Non-orientable Manifolds, and Anomalies, *Commun. Math. Phys.* **374**, 1021 (2020).

[42] E. Verlinde, Fusion rules and modular transformations in 2D conformal field theory, *Nucl. Phys. B* **300**, 360 (1988).

[43] G. Moore and N. Seiberg, Classical and quantum conformal field theory, *Commun. Math. Phys.* **123**, 177 (1989).

[44] Y. Hu, S. D. Stirling, and Y.-S. Wu, Emergent exclusion

statistics of quasiparticles in two-dimensional topological phases, *Phys. Rev. B* **89**, 115133 (2014).

[45] A. Kitaev, Anyons in an exactly solved model and beyond, *Ann. Phys. (NY)* **321**, 2 (2006).

[46] S. H. Simon, *Topological Quantum* (Oxford University Press, 2023).

[47] Z. Nussinov and G. Ortiz, A symmetry principle for topological quantum order, *Ann. Phys. (NY)* **324**, 977 (2009).

[48] A. Ritz-Zwilling, J.-N. Fuchs, and J. Vidal, Wegner-Wilson loops in string nets, *Phys. Rev. B* **103**, 075128 (2021).

[49] M. D. Schulz, S. Dusuel, K. P. Schmidt, and J. Vidal, Topological Phase Transitions in the Golden String-Net Model, *Phys. Rev. Lett.* **110**, 147203 (2013).

[50] A. Schotte, J. Carrasco, B. Vanhecke, L. Vanderstraeten, J. Haegeman, F. Verstraete, and J. Vidal, Tensor-network approach to phase transitions in string-net models, *Phys. Rev. B* **100**, 245125 (2019).

[51] M. B. Hastings and X.-G. Wen, Quasiadiabatic continuation of quantum states: The stability of topological ground-state degeneracy and emergent gauge invariance, *Phys. Rev. B* **72**, 045141 (2005).

[52] A. Kitaev and J. Preskill, Topological Entanglement Entropy, *Phys. Rev. Lett.* **96**, 110404 (2006).

[53] M. A. Levin and X.-G. Wen, Detecting Topological Order in a Ground State Wave Function, *Phys. Rev. Lett.* **96**, 110405 (2006).

[54] A. Hamma, R. Ionicioiu, and P. Zanardi, Ground state entanglement and geometric entropy in the Kitaev's model, *Phys. Lett. A* **337**, 22 (2005).

[55] S. Iblisdir, D. Pérez-García, M. Aguado, and J. Pachos, Scaling law for topologically ordered systems at finite temperature, *Phys. Rev. B* **79**, 134303 (2009).

[56] S. Iblisdir, D. Pérez-García, M. Aguado, and J. Pachos, Thermal states of anyonic systems, *Nucl. Phys. B* **829**, 401 (2010).

[57] M. Hermanns and S. Trebst, Renyi entropies for classical string-net models, *Phys. Rev. B* **89**, 205107 (2014).

[58] Z. Weinstein, G. Ortiz, and Z. Nussinov, Universality Classes of Stabilizer Code Hamiltonians, *Phys. Rev. Lett.* **123**, 230503 (2019).

[59] T. Neupert, H. He, C. von Keyserlingk, G. Sierra, and B. A. Bernevig, Boson condensation in topologically ordered quantum liquids, *Phys. Rev. B* **93**, 115103 (2016).

[60] N. Bultinck, M. Mariën, D. J. Williamson, M. B. Şahinoğlu, J. Haegeman, and F. Verstraete, Anyons and matrix product operator algebras, *Ann. Phys. (NY)* **378**, 183 (2017).

[61] C. Delcamp, B. Dittrich, and A. Riello, Fusion basis for lattice gauge theory and loop quantum gravity, *J. High Energy Phys.* **2017**, 61.

[62] E. Rowell, R. Stong, and Z. Wang, On classification of modular tensor categories, *Commun. Math. Phys.* **292**, 343 (2009).

[63] R. E. Gompf and A. I. Stipsicz, *4-Manifolds and Kirby Calculus*, Graduate Studies in Mathematics, Vol. 20 (AMS, 1999).

[64] R. C. Kirby, *The Topology of 4-Manifolds*, Lecture Notes in Mathematics, Vol. 1374 (Springer, 1980).

[65] W. B. R. Lickorish, A representation of orientable combinatorial 3-manifolds, *Ann. Math.* **76**, 531 (1962).

[66] W. B. R. Lickorish, Homeomorphisms of non-orientable two-manifolds, *Mathematical Proceedings of the Cambridge Philosophical Society* **59**, 307–317 (1963).

[67] A. H. Wallace, Modifications and cobounding manifolds, *Canadian Journal of Mathematics* **12**, 503–528 (1960).

[68] E. Witten, Quantum field theory and the Jones polynomial, *Commun. Math. Phys.* **121**, 351 (1989).

[69] N. Reshetikhin and V. G. Turaev, Invariants of 3-manifolds via link polynomials and quantum groups, *Invent. Math.* **103**, 547 (1991).